Table 3
Strategies to overcome the heterogeneity of the EPR effect, and augmentation of the EPR effect to enhance tumor drug delivery.[a]

Methods[a]	Mechanism	Remarks
1. Use of angiotensin II-induced hypertension	Hydrodynamic; vasoconstriction induced hypertension → mechanical opening of endothelial cell-cell gaps passively.	Drug is infused into the tumor-feeding artery via cathether.
2. Use of angiotensin I-converting enzyme (ACE) inhibitor such as enalapril	Selectively elevates the kinin level only in tumors, by inhibiting kinin degradation by ACE-inhibitor, which occurs in the tumor tissue.	Given orally, very safe, clinically proven.
3. Use of nitroglycerin given topically by dermal patch, or by infusion via the tumor-feeding artery	Generates NO in hypoxic tumor issue selectively. See analogy to angina pectoris.	Nitroglycerin, isosorbide dinitrate (ISDN, Nitrol®), nitroprusside, and others; clinically proven (see text).
4. Use of prostaglandin (PG) I_2 analogue, beraprost sodium	PG agonist effect (with the $t_{1/2}$ more than 100 times longer in plasma) when given orally.	
5. Use of TGF-β-inhibitor	TGF-β is tumor growth and differentiation factor. Facilitate productive of extracellular matrix. The inhibitor counteracts to restore vascular maturation and normalization, which may be affected by vascular mediator.	Shown effective in the pancreatic cancer in vivo model.
6. Use induction of HO-1, or a CO generator (ruthenium tri carbonyl, CORM2[b])	Zn protoporphyrin or hemin–polymer conjugates induce HO-1 in tumors; use of CORM2 generates CO. See text.	No data available for in vivo therapeutic efficacy.

[a] These strategies will be effective only with nanoparticle or polymeric drugs.
[b] Carbon monoxide-releasing molecule.

concentration in plasma [15–21]; (iii) no immunogenicity [15]; and (iv) higher lipophilicity, which enabled solubilization and formulation with a lipid contrast agent (Lipiodol®) as a carrier (i.e., the SMANCS/Lipiodol formulation) [14,18,21–25]. This lipid formulation allowed truly selective tumor targeting and tumor delivery by infusion into the tumor-feeding artery via a catheter under X-ray guidance of angiographic technique as viewed on the monitoring screen [21–25]. A drug concentration in the tumor as much as 2000 times the concentration in blood (2000:1) can be achieved by using this method [22]. The EPR effect is now known to allow most macromolecular drugs to be selectively delivered to solid tumors, where they remain for very long periods, several weeks or months or even more [16,18,21–25]. This sustained drug activity will result in a marked therapeutic effect [18,22–24].

3. Advancements in tumor targeting with SMANCS/Lipiodol via the i.a. route

We have now extended the application of SMANCS/Lipiodol therapy, administered via i.a. infusion, to advanced, difficult-to-treat solid tumors such as massive and multiple metastatic liver cancers, bile duct carcinomas and cholangiocarcinomas, and pancreatic cancers and their metastatic nodules in the liver [24]. We also successfully treated massive renal cell cancer similarly, by infusion into the renal artery. Descriptions of these examples have been published [18,25]. In this article, we provide examples of such augmented drug delivery, by means of angiotensin II-induced high blood pressure, to advanced, difficult-to-treat tumors: pancreatic cancer with metastatic liver cancer (Fig. 1A and B), and metastatic liver cancer that had originated from gastric cancer, which had previously been removed (Fig. 1C and D).

For both cases, we infused SMANCS/Lipiodol i.a. under conditions of angiotensin II-induced high blood pressure (e.g., from 100 mm Hg to 150 mm Hg) [25]. The blood pressure of 150–160 mm Hg was achieved via slow i.v. infusion of 0.5 μg/ml angiotensin II, that is set in a 20 ml infusion syringe-pump. This method offers not only an improved therapeutic effect but also a diagnostic value, given the highly sensitive detection, by means of computed tomography (CT), of the tumor-selective uptake of Lipiodol, even in small tumor nodules with diameters of 3–5 mm. Another advantage of using angiotensin II-induced high blood pressure is application to more types of tumors that may be treated by this method. In fact almost all cases responded very well (25). Under normotension, as SMANCS/Lipiodol was originally used, the drug was most effective for primary liver cancer (hepatocellular carcinoma) but was less effective for metastatic liver cancer and cholangiocarcinoma. The reason for this difference may be poor drug delivery to the tumor because of the heterogeneity of the EPR effect. As Fig. 1 shows, the improved delivery method that utilizes angiotensin II-induced high blood pressure indeed makes SMANCS/Lipiodol highly effective. Another benefit of this method is the reduced time required for tumor regression (e.g., to achieve 50% of tumor volume), perhaps because of increased targeted drug delivery, and with less frequent drug administration needed.

4. Heterogeneity of the EPR effect, which hinders tumor delivery, and the method of circumventing this heterogeneous drug delivery [16–18]

Although the EPR effect offers the first step in the process of delivering drugs to tumor tissue or near tumor cells, solid tumors in clinical settings frequently have heterogeneous characteristics as described in Section 1, and some tumors impede drug access to tumors because of necrosis, fibrosis, clot formation, or interference by stromal tissue [16,17,26,27]. However, in the past several years, we have devised ways, by means of different techniques, to improve this process of drug delivery to such tumors, as described below and as shown in Table 3.

4.1. Induced hypertension by using a slow i.v. infusion of angiotensin II

Inducing hypertension via a slow i.v. infusion of angiotensin II [21,25,28,29] is more useful for macromolecular drugs and drug/Lipiodol formulations given during arterial infusion than for low-MW drugs. This method was briefly described above (Section 3). Low-MW drugs offer little advantage in this method, perhaps because of rapid diffusion or washout [29].

4.2. Using nitroglycerin or other nitric oxide (NO)-releasing agents

Nitroglycerin and other NO-releasing agents generate NO from NO_2^- selectively in hypoxic tumor tissue compared with normoxic tissues [30,31]. Thus, such nitro agents facilitate the EPR effect via local NO generation in tumors, with drug delivery enhanced 2- to 3-fold and an improved therapeutic effect. Yasuda et al. [32,33] and Siemens et al. [34] also demonstrated the beneficial effect of NO-releasing agents used in combination with conventional low-MW drugs. In this review, I describe clinical cases of bronchogenic lung cancer for which isosorbide dinitrate (ISDN), an NO-releasing agent, was administered 50–100 μg in 1–2 ml of physiological saline, bolus, via the bronchial artery immediately before SMANCS/Lipiodol infusion into the same bronchial artery (see Section 6).

4.3. Using an angiotensin-converting enzyme inhibitor (ACEI)

Solid tumors generate bradykinin, which would aid the EPR effect. ACEIs inhibit the degradation of bradykinin, thus raising the local bradykinin concentration in tumor tissue more than in other tissues in the body [16,17,26]. For example, use of the combination of an ACEI and hypertension improved monoclonal antibody delivery 2- to 3-fold

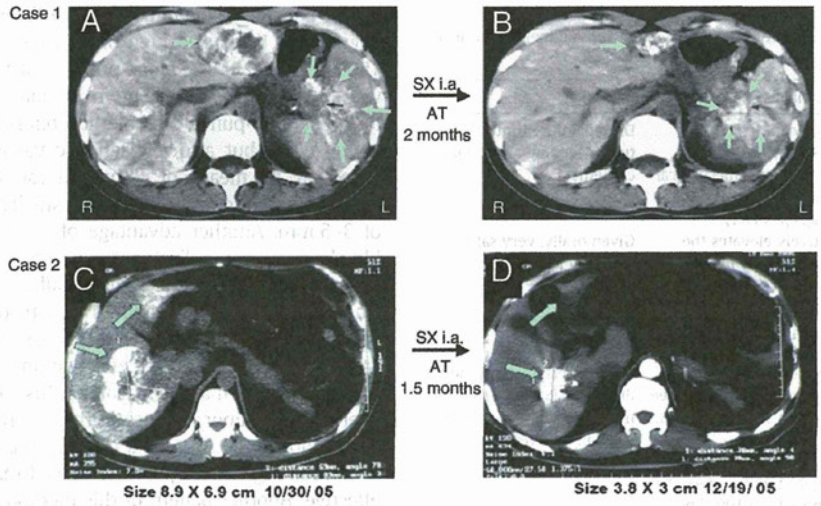

Fig. 1. Cases 1 and 2. Therapeutic effect of SMANCS/Lipiodol against advanced, difficult-to-treat cancers. The drug was infused via the tumor-feeding artery (hepatic artery) under angiotensin II-induced high blood pressure. A and C are abdominal CT scans 2 days after drug infusion. B and D are CT scans taken 2 and 1.5 months after drug infusion, respectively. Case 1. Pancreatic cancer with metastatic liver cancer (A) regressed significantly after 2 months. (B) Remarkable reduction in the size of the metastatic liver cancer (top, right). Case 2. Gastric cancer had metastasized to the liver (C). The two visible large tumor foci evidenced a marked size reduction after 1.5 months (D). White areas in the CT scans, other than bones, indicate where SMANCS/Lipiodol was selectively taken up by the tumors; other (normal) areas did not take up the drug (see the text for a description of the procedure). From Ref. [25].

in a xenograft mouse model of human gastric cancer [26,35]. This method was also validated effective by Dr. F. Kratz of Freiburg in different tumor model (personal communication).

4.4. Generating carbon monoxide (CO)

Fang et al. in our laboratory described the important role of heme oxygenase 1 (HO-1) in the EPR effect which is upregulated in most solid tumors; its product, CO, was also a factor influencing the EPR effect. CO has a physiological role similar to the vasodilator role of NO, so it will also have a key function in the EPR effect [36]. Thus, upregulation of HO-1 by HO-1 inducers such as pegylated hemin or similar agents, or CO-releasing agents (e.g., carbon monoxide-releasing molecule, CORM2), can facilitate the EPR effect [17,36].

5. Drug access to tumor cells and cellular drug uptake, followed by reaction of active drug with target molecules in tumor cells

Although nanoparticles can get to tumor tissues by means of the EPR effect, other issues complicating efficient drug uptake remain to be cleared. These issues include access of drugs to tumor cells and internalization of drugs, followed by release of the free or active drugs from macromolecular formulations composed of liposomes, micelles, or polymer conjugates such as polyethylene glycol (PEG), *N*-(2-hydroxyproply)methacrylamide (HPMA), or SMA. Achieving efficient drug uptake requires knowledge of tumor biology, such as targeting to unique receptors, making use of higher lipophilicity, and utilizing a unique ligand with high affinity to tumor cell receptors of a particular tumor. With regard to uptake of nanoparticle-drugs into tumor cells, in many cases cancer cells have more active endocytic uptake than do dormant normal cells.

Cellular drug uptake is more efficient with SMA micelles than with PEG-micelles [37 and our unpublished data]. For example, when we evaluated SMANCS and NCS, SMANCS was much more toxic to tumor cells than to normal cells [38]. Also, to kill 80% of the cells, NCS required more than 1 h at 30 nM, whereas SMANCS required only a few minutes at 15 nM [38]. Furthermore, a recent comparison of SMA-Zn protoporphyrin (PP) micelles and PEG–ZnPP micelles showed a more rapid cellular uptake for the former [37]. SMA–ZnPP micelles also demonstrated rapid uptake by tumor cells, with very quick disintegration of the micellar structure in the cells. Thus, release of free drug, ZnPP upon rapid endocytic uptake of SMA-ZnPP into tumor cells is anticipated [37]. Then, the free active drugs would be expected to react with target molecules in the cells (unpublished data).

6. Obstacles in drug development, drug promotion, and decision-making in business: dilemmas for science and business

6.1. Novel drug administration technique for use at the bedside

The first obstacle that we encountered in clinical drug development concerned the method of drug administration: the route via the tumor-feeding artery. In cardiology, the angiographic technique for imaging, which utilizes arterial infusion of a contrast agent to visualize an occluded artery and damaged tissue, is a routine practice in major hospitals. The same technique has been used much less frequently or very rarely in cancer treatment, although interventional radiologists utilize it, primarily for embolization of the tumor-feeding artery so as to achieve tumor necrosis, with limited effects [39].

In SMANCS/Lipiodol therapy, the lipid formulation of SMANCS is infused into the tumor-feeding artery—the hepatic artery for hepatoma, the renal artery for cancer of the kidney, and the bronchial artery for lung cancer or bronchogenic cancer (Figs. 1–3) [18,23,25]. This infusion occurs simultaneously with angiographic imaging of the tumor, with identification of the tumor-feeding artery. This technique requires adequate skill to manipulate the catheter under X-ray guidance, more skill than that needed for the commonly used i.v. infusion, and not every health care professional can perform such drug administration. Also, some pharmaceutical companies do not view such an elaborate method favorably, so it becomes a negative incentive for a business undertaking. However, this perception may be reversed when members of top management of a company carefully examine and investigate the positive clinical outcomes. For example, organizing a task force to promote this therapeutic modality using SMANCS/Lipiodol may encourage opening of a new market.

6.2. Market size: $n \times T$ dominates the corporate decision

The second obstacle to developing new candidate drugs, which is usually the first question that people ask us, is, how big will the market

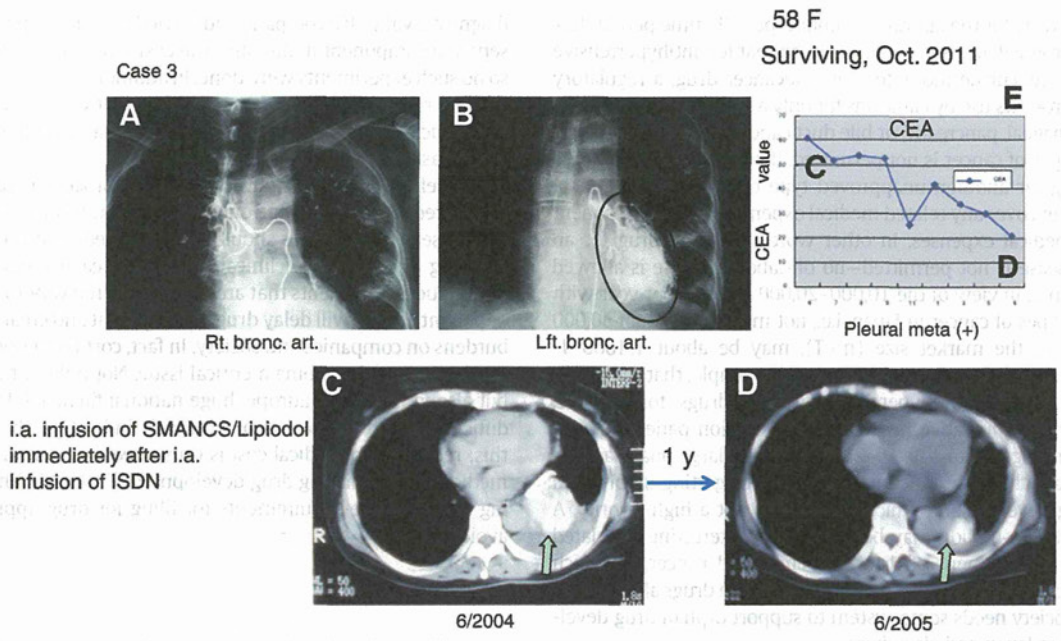

Fig. 2. Case 3. Lung cancer (adenocarcinoma). A and B are angiograms showing infusion of contrast agent into the right bronchial artery (A) and left bronchial artery (B). These X-ray images indicate that the tumor is fed by two different arteries. (C) Initial CT scan at the start of treatment (arrow shows tumor area). (D) CT scan showing considerable tumor regression (arrow) after 1 year. SMANCS/Lipiodol, about 0.5 ml (mg), was infused into each bronchial artery immediately after infusion of a microdose of Nitrol (10–50 μg/dose). (D) One year after treatment, the tumor in the pleural cavity is considerably smaller. White areas indicate remaining drug. (E) Graph showing the decrease in the tumor marker CEA (carcinoembryonic antigen); C and D in [E] correspond to the CT scans in C and D.

be? When we began the clinical application of SMANCS/Lipiodol to treat hepatoma in Japan in the 1980s, about 20,000 cases occurred per year, which by 2010 had increased to about 33,000. In the United States, the corresponding number in the 1980s was about 10,000, although it is much larger now, which was not a favorable size for drug development. In addition, not all of 10,000 patients would be using SMANCS so that actual market size would be far smaller.

Today in Japan, almost 500,000 new cancer cases arise annually. However, in contrast to the number of cancer patients, the number of patients in Japan with diabetes mellitus, hypertension, hypercholesterolemia, and osteoporosis, which are the primarily chronic diseases, exceeds several million. In addition, cancer patients require a much shorter period of drug administration compared with patients with those chronic diseases. Therefore, for anticancer drugs, the product of n (number of patients

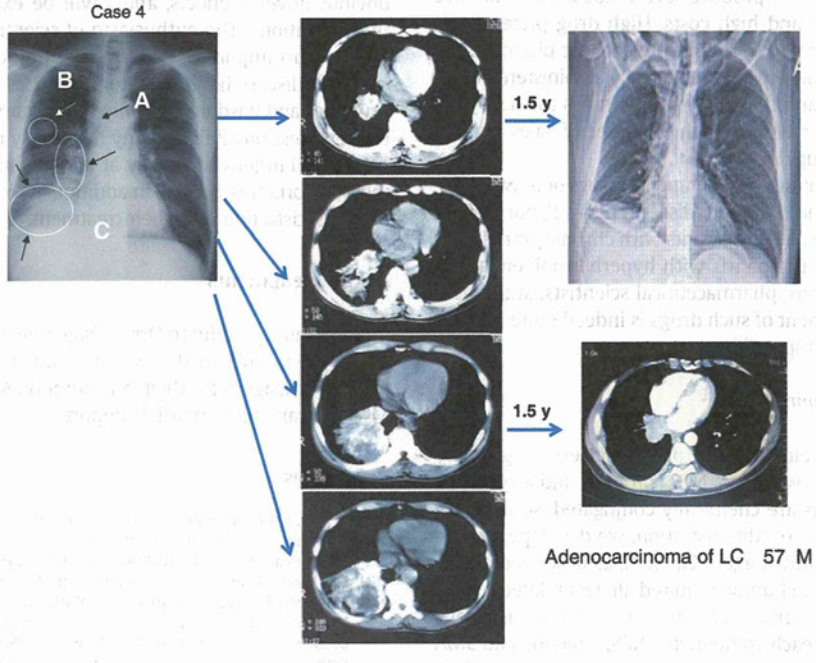

Fig. 3. Case 4. Lung adenocarcinoma. (Top left) Initial chest X-ray showing multiple tumors A, B, and C (circled areas, arrows). The patient underwent Nitrol infusion followed by SMANCS/Lipiodol infusion of 0.5 mg/0.5 ml into both bronchial arteries, as in Case 3. (Middle) CT scans from the subscapular to the lower pleural cavity at the time of initial infusion. (Right) Both chest X-ray (top) and CT scan (bottom) show remarkable tumor regression after 1.5 years; and the patient had no subjective complaints during this period.

eligible to use a drug for the approved tumor type)×T (time period during which the drug will be used) is far less than that for antihypertensive drugs, for instance. Furthermore, for any anticancer drug, a regulatory agency will approve its use by clinicians for only a specific type of cancer, e.g., brain, esophageal, pancreatic, or bile duct cancer individually, and its use for other types of cancer is not permitted. If a clinician in Japan prescribes the drug for another, unapproved type of cancer, the national insurance will not cover any related medical expenses, so that the patient must pay all medical expenses. In other words, use of a drug for an unapproved disease is not permitted—no off-label drug use is allowed in Japan. Therefore, in view of the 10,000–20,000 patients per year with many of these types of cancer in Japan, i.e., not much more than 50,000 patients per year, the market size (n×T), may be about 1/1000–1/10,000 for each cancer type, compared with, for example, that for statins (anticholesterol agents). Antihypercholesterolemic drugs, for instance, were obviously more lucrative because several million patients would use them for far longer than, say, 10–20 years. Many large pharmaceutical companies are therefore less enthusiastic about getting involved in anticancer drug development, which for them is not a high priority. A market size of half-a-million may be moderately interesting. A related issue concerns development of drugs for childhood cancer, in which there is not much interest. The development of orphan drugs also lags behind need, so society needs some system to support orphan drug development as well in Japan and elsewhere.

When SMANCS/Lipiodol was first demonstrated to be very effective against liver cancer, the market size in the United States was small, about 10,000, and the potential market for this drug was not so lucrative. The company that was developing SMANCS/Lipiodol in Japan also did little to promote the drug, regardless of its advantages—remarkable clinical benefits and very few adverse effects. Such decisions depend on the policies of each individual pharmaceutical company, and unfortunately, the executives of the company developing SMANCS/Lipiodol did not see the potential impact of this drug in Japan or elsewhere. In addition, this therapeutic strategy, which would have stimulated a paradigm change in solid tumor treatment as described earlier herein, would have stimulated the growth of a new market for use of this agent to treat other solid cancers.

With regard to the cost/benefit issue for cancer patients, many conventional anticancer drugs usually produce severe side effects but have marginal therapeutic efficacy and high costs. High drug prices mean that the drugs will be highly profitable and lucrative for the pharmaceutical companies. SMANCS/Lipiodol, however, is usually administered three to five times in the first year, and then two or three times the next year. This administration schedule means that the number of sales is quite small, which thus impedes drug development.

We have discovered very interesting therapeutic drugs or new modalities for treatment of cancer and other rare diseases [39–42], but making such drugs or modalities available for patients with chronic granulomatous disease [41] or fulminant hepatitis with hyperbilirubinemia [43] requires enthusiastic physicians, pharmaceutical scientists, and industrialists. In practice, development of such drugs is indeed quite difficult or almost, if not completely, impossible.

6.3. Regulation in drug development

The third obstacle to developing new drugs concerns regulatory agencies. SMANCS consists of two parts: NCS (protein) and a synthetic copolymer of SMA. Both parts are chemically conjugated, so the drug is a single chemical entity. For its administration, we developed a new formulation with the lipid contrast agent Lipiodol, as described above. However, a regulatory agency in Europe required all data related to toxicity, pharmacokinetics, and pharmacodynamics, as well as clinical data, to be provided separately for each component: NCS, Lipiodol, and SMA copolymer, (the latter two have no cytotoxic or anticancer activity). Our preclinical data in rodents showed that only the SMANCS in Lipiodol formulation demonstrated the far greater therapeutic benefit as well as diagnostic value. If a company had carried out such experiments for each separate component in humans, the cost would have been prohibitory, so no such experiments were done. In addition, my colleague physicians, with no reason to believe that clinical benefit would ensue, objected to doing such unethical clinical studies of humans, with legal actions following as the worst outcome.

Therefore, during the filing for approval process, regulatory agencies should require and examine only preclinical and clinical data of the drug being used. The agencies should be concerned with the formulation of the drug as used in the clinical setting, not each separate component. To conduct experiments that are not directly relevant to clinical practice or patient benefit will delay drug development and create great financial burdens on companies and society. In fact, cost reduction in drug development is now becoming a critical issue. Not only in the United States but also in Japan and Europe, huge national financial debts are causing difficulties, and medical expenditure is indeed partly responsible for this; reduction in medical cost is thus a requirement in every aspect of medical care, including drug development [7–10,44]. Therefore, imposing unreasonable requirements for filing for drug approval should be avoided [7,8].

7. Conclusion

In this article, I describe my personal experiences with the EPR effect and development of macromolecular therapeutics (SMANCS), including marketing issues. Essential focal points of development of such drugs involve the cost of the drug and its efficacy. Price setting is a complex issue: if a price is too low, a company will lose interest, but if it is too high, society will suffer. Furthermore, in the current arena of anticancer drug development, the need for a wide range of knowledge about cancer genomics and cancer biology is not fully appreciated. Drug development based on the EPR effect is certainly an important first step, but some problems still remain. Even after a drug is delivered to cancer tissue, it must be taken up by tumor cells, and free active drug must then be released and interact with target molecules. The case of SMA–ZnPP micelles serves as an example of such a drug in development. Also, the heterogeneity of the EPR effect must be overcome. I have addressed this heterogeneity and achieved realistic in vivo solutions that have no obvious adverse effects, and I will be excited when clinicians adopt these solutions. The enthusiasm of scientists as well as industry is by far the most important key for successful drug development.

I also discuss how regulatory agencies should act responsibly, with prudence and wisdom, not only with regard to safety issues, even when the remotest possibility of any harm may exist, but also with regard to economic burdens to society at large. Clinical efficacy is, of course, the most important issue, and in addition, patients should display a high degree of satisfaction with their treatment.

Acknowledgments

I am most grateful to Drs. A. Nagamitsu and K. Greish for permitting me to use unpublished Figs. 2 and 3. I also thank all my previous and present colleagues for their collaboration Ms. J.B. Gandy for editing, and Ms. A. Takaki for secretarial support.

References

[1] C. Leaf, Why we're losing the war on cancer, Fortune 149 (2004) 76–97.
[2] G.L. Gabor Miklos, The human cancer genome project—one more misstep in the war on cancer, Nat. Biotechnol. 23 (2005) 535–537.
[3] L.D. Wood, D.W. Parsons, S. Jones, J. Lin, T. Sjöblom, R.J. Leary, D. Shen, S.M. Boca, T. Barber, J. Ptak, N. Silliman, S. Szabo, Z. Dezso, V. Ustyanksky, T. Nikolskaya, Y. Nikolsky, R. Karchin, P.A. Wilson, J.S. Kaminker, Z. Zhang, R. Croshaw, J. Willis, D. Dawson, M. Shipitsin, J.K. Willson, S. Sukumar, K. Polyak, B.H. Park, C.L. Pethiyagoda, P.V. Pant, D.G. Ballinger, A.B. Sparks, J. Hartigan, D.R. Smith, E. Suh, N. Papadopoulos, P. Buckhaults, S.D. Markowitz, G. Parmigiani, K.W. Kinzler, V.E. Velculescu, B. Vogelstein, The genomic landscapes of human breast and colorectal cancers, Science 318 (2007) 1108–1113.

[4] T. Sjöblom, S. Jones, L.D. Wood, D.W. Parsons, J. Lin, T.D. Barber, D. Mandelker, R.J. Leary, J. Ptak, N. Silliman, S. Szabo, P. Buckhaults, C. Farrell, P. Meeh, S.D. Markowitz, J. Willis, D. Dawson, J.K. Willson, A.F. Gazdar, J. Hartigan, L. Wu, C. Liu, G. Parmigiani, B.H. Park, K.E. Bachman, N. Papadopoulos, B. Vogelstein, K.W. Kinzler, V.E. Velculescu, The consensus coding sequences of human breast and colorectal cancers, Science 314 (2006) 268–274.
[5] R. Mayer, Targeted therapy for advanced colorectal cancer—more is not always better, N. Engl. J. Med. 360 (2009) 623–625.
[6] S.P. Shah, R.D. Morin, J. Khattra, L. Prentice, T. Pugh, A. Burleigh, A. Delaney, K. Gelmon, R. Guliany, J. Senz, C. Steidl, R.A. Holt, S. Jones, M. Sun, G. Leung, R. Moore, T. Severson, G.A. Taylor, A.E. Teschendorff, K. Tse, G. Turashvili, R. Varhol, R.L. Warren, P. Watson, Y. Zhao, C. Caldas, D. Huntsman, M. Hirst, M.A. Marra, S. Aparicio, Mutation evolution in a lobular breast tumor profiled at single nucleotide resolution, Nature 461 (2009) 809–813.
[7] Anonymous, Editorial, Welcome clinical leadership at NICE, Lancet 372 (2008) 601.
[8] Story from BBC News, Liver cancer drug 'too expensive', http://news.bbc.co.uk/2/hi/health/8367614.stm.
[9] K. Baicker, M.E. Chernew, The economics of financing Medicare, N. Engl. J. Med. 365 (4) (2011) e7.
[10] T. Fojo, C. Grady, How much is life worth: cetuximab, non-small cell lung cancer, and the $440 billion question, J. Natl. Cancer Inst. 101 (2009) 1044–1048.
[11] W.J. Chng, L.A. Loeb, J.H. Bielas, Limits to the human cancer genome project? Science 315 (2007) 762–764.
[12] J. Tol, M. Koopman, A. Cats, C.J. Rodenburg, G.J. Creemers, J.G. Schrama, F.L. Erdkamp, A.H. Vos, C.J. van Groeningen, H.A. Sinnige, D.J. Richel, E.E. Voest, J.R. Dijkstra, M.E. Vink-Börger, N.F. Antonini, L. Mol, J.H. van Krieken, O. Dalesio, C.J. Punt, Chemotherapy, bevacizumab, and cetuximab in metastatic colorectal cancer, N. Engl. J. Med. 360 (2009) 563–572.
[13] H. Maeda, J. Takeshita, R. Kanamaru, A lipophilic derivative of neocarzinostatin: a polymer conjugation of an antitumor protein antibiotic, Int. J. Pept. Protein Res. 14 (1979) 81–87.
[14] H. Maeda, M. Ueda, T. Morinaga, T. Matsumoto, Conjugation of poly(styrene-co-maleic acid) derivatives to the antitumor protein neocarzinostatin: pronounced improvements in pharmacological properties, J. Med. Chem. 28 (1985) 455–461.
[15] H. Maeda, T. Matsumoto, T. Konno, K. Iwaki, M. Ueda, Tailor-making of protein drugs by polymer conjugation for tumor targeting: a brief review on Smancs, J. Protein Chem. 3 (1984) 181–193.
[16] H. Maeda, Tumor-selective delivery of macromolecular drugs via the EPR effect: background and future prospects, Bioconjug. Chem. 21 (2010) 797–802.
[17] J. Fang, H. Nakamura, H. Maeda, EPR effect: the unique characteristics of tumor blood vessels for drug delivery, factors involved, its limitation and augmentation, Adv. Drug Deliv. Rev. 63 (2011) 136–151.
[18] H. Maeda, Enhanced permeability and retention effect in relation to tumor targeting, in: F. Kratz, P. Senter, H. Steinhagen (Eds.), Drug Delivery in Oncology. From Basic Research to Cancer Therapy, Wiley-VCH Verlag GmbH & Co. KG, Weinheim, Germany, 2011, pp. 65–84.
[19] K. Hochdörffer, G.D. Stefano, H. Maeda, F. Kratz, Liver tumor targeting, in: F. Kratz, P. Senter, H. Steinhagen (Eds.), Drug Delivery in Oncology. From Basic Research to Cancer Therapy, Wiley-VCH Verlag GmbH & Co. KG, Weinheim, Germany, 2011, pp. 1519–1568.
[20] Y. Matsumura, H. Maeda, A new concept for macromolecular therapeutics in cancer chemotherapy: mechanism of tumoritropic accumulation of proteins and the antitumor agent SMANCS, Cancer Res. 46 (1986) 6387–6392.
[21] H. Maeda, T. Sawa, T. Konno, Mechanism of tumor-targeted delivery of macromolecular drugs, including the EPR effect in solid tumor and clinical overview of the prototype polymeric drug SMANCS, J. Control. Release 74 (2001) 47–61.
[22] K. Iwai, H. Maeda, T. Konno, Use of oily contrast medium for selective drug targeting to tumor: enhanced therapeutic effect and X-ray image, Cancer Res. 44 (1984) 2115–2121.
[23] T. Konno, H. Maeda, K. Iwai, S. Maki, S. Tashiro, M. Uchida, Y. Miyauchi, Selective targeting of anti-cancer drug and simultaneous image enhancement in solid tumors by arterially administered lipid contrast medium, Cancer 54 (1984) 2367–2374.
[24] S. Maki, T. Konno, H. Maeda, Image enhancement in computerized tomography for sensitive diagnosis of liver cancer and semiquantitation of tumor selective drug targeting with oily contrast medium, Cancer 56 (1985) 751–757.
[25] A. Nagamitsu, K. Greish, H. Maeda, Elevating blood pressure as a strategy to increase tumor targeted delivery of macromolecular drug SMANCS: cases of advanced solid tumors, Jpn. J. Clin. Oncol. 39 (2009) 756–766.
[26] H. Maeda, Vascular permeability in cancer and infection as related to macromolecular drug delivery, with emphasis on the EPR effect for tumor-selective drug targeting, Proc. Jpn. Academy, Series B. 88 (2012) 53–71.
[27] J. Daruwalla, M. Nikfarjam, K. Greish, C. Malcontenti-WilsonI, V. Muralidharan, C. Christophi, H. Maeda, In vitro and in vivo evaluation of tumor targeting SMA–pirarubicin micelles: survival improvement and inhibition of liver metastases, Cancer Sci. 101 (2010) 1866–1874.
[28] M. Suzuki, K. Hori, I. Abe, S. Saito, H. Sato, A new approach to cancer chemotherapy: selective enhancement of tumor blood flow with angiotensin II, J. Natl. Cancer Inst. 67 (1981) 663–669.
[29] C.J. Li, Y. Miyamoto, Y. Kojima, H. Maeda, Augmentation of tumour delivery of macromolecular drugs with reduced bone marrow delivery by elevating blood pressure, Br. J. Cancer 67 (1993) 975–980.
[30] H. Maeda, Nitroglycerin enhances vascular blood flow and drug delivery in hypoxic tumor tissues: analogy between angina pectoris and solid tumors and enhancement of the EPR effect, J. Control. Release 142 (2010) 296–298.
[31] T. Seki, J. Fang, H. Maeda, Enhanced delivery of macromolecular antitumor drugs to tumors by nitroglycerin application, Cancer Sci. 100 (2009) 2426–2430.
[32] H. Yasuda, M. Yamaya, K. Nakayama, T. Sasaki, S. Ebihara, A. Kanda, M. Asada, D. Inoue, T. Suzuki, T. Okazaki, H. Takahashi, M. Yoshida, T. Kaneta, K. Ishizawa, S. Yamanda, N. Tomita, M. Yamasaki, A. Kikuchi, H. Kubo, H. Sasaki, Randomized phase II trial comparing nitroglycerin plus vinorelbine and cisplatin with vinorelbine and cisplatin alone in previously untreated stage IIIB/IV non-small cell lung cancer, J. Clin. Oncol. 24 (2006) 688–694.
[33] H. Yasuda, K. Nakayama, M. Watanabe, S. Suzuki, H. Fuji, S. Okinaga, A. Kanda, K. Zayazu, T. Sasaki, M. Asada, T. Suzuki, M. Yoshida, S. Yamanda, D. Inoue, T. Kaneta, T. Kondo, Y. Takai, H. Sasaki, K. Yanagihara, M. Yamaya, Nitroglycerin treatment may increase response to docetaxel and carboplatin regimen via inhibitions of hypoxia-inducible factor-1 pathway and P-glycoprotein in patients with lung adenocarcinoma, Clin. Cancer Res. 12 (2006) 6748–6757.
[34] D.R. Siemens, J.P.W. Heaton, M.A. Adams, J. Kawakami, C.H. Graham, Phase II study of nitric oxide donor for men with increasing prostate-specific antigen level after surgery or radiotherapy for prostate cancer, Urology 74 (2009) 878–883.
[35] A. Noguchi, T. Takahashi, T. Yamaguchi, K. Kitamura, A. Noguchi, H. Tsurumi, K. Takashina, H. Maeda, Enhanced tumor localization of monoclonal antibody by treatment with kininase II inhibitor and angiotensin II, Jpn. J. Cancer Res. 83 (1992) 240–243.
[36] J. Fang, H. Qin, H. Nakamura, K. Tsukigawa, H. Maeda, Carbon monoxide, generated by heme oxygenase-1, mediates the enhanced permeability and retention (EPR) effect of solid tumor, Cancer Sci. 102 (2012) 535–541.
[37] H. Nakamura, J. Fang, B. Gahininath, K. Tsukigawa, H. Maeda, Intracellular uptake and behavior of two types zinc protoporphyrin (ZnPP) micelles, SMA–ZnPP and PEG–ZnPP as anticancer agents; unique intracellular disintegration of SMA micelles, J. Control. Release 155 (2011) 367–375.
[38] T. Oda, F. Sato, H. Yamamoto, M. Akagi, H. Maeda, Cytotoxicity of smancs in comparison with other anticancer agents against various cells in culture, Anticancer Res. 9 (1989) 261–266.
[39] R. Avtister, J. Wallace, Interventional radiology for the cancer patient, in: W.K. Hong, R.C. Bast, W.N. Hait, D.W. Kufe, R.E. Pollock, R.R. Weichelbaum; J.F. Holland, E. Frei (Eds.), Holland-Frei Cancer Medicine, 8th edition, People's Medical Publishing House—USA, Shelton, CT, 2010, pp. 490–497.
[40] T. Sawa, J. Wu, T. Akaike, H. Maeda, Tumor-targeting chemotherapy by a xanthine oxidase–polymer conjugate that generates oxygen-free radicals in tumor tissue, Cancer Res. 60 (2000) 666–671.
[41] J. Fang, H. Qin, T. Seki, H. Nakamura, K. Tsukigawa, H. Maeda, Therapeutic potential of pegylated hemin for ROS-related diseases via induction of heme oxygenase-1: results from a rat hepatic ischemia/reperfusion injury model, J. Pharmacol. Exp. Ther. 339 (2011) 779–789.
[42] H. Nakamura, J. Fang, H. Maeda, Protective role of D-amino acid oxidase against bacterial infection, Infect. Immun. 80 (2012) 1546–1553.
[43] M. Kimura, Y. Matsumura, Y. Miyauchi, H. Maeda, A new tactic for the treatment of jaundice: an injectable polymer-conjugated bilirubin oxidase, Proc. Soc. Exp. Biol. Med. 188 (1988) 364–369.
[44] P.B. Ginsburg, C. White, Health care's role in deficit reduction — guiding principles, N. Engl. J. Med. 365 (2011) 1559–1561.

EPR効果に基づく腫瘍のターゲッティングと蛍光イメージング

前田　浩

崇城（そうじょう）大学DDS研究所

1. はじめに

EPR効果は癌のDDSを考える上で最も重要なfindingと言われているが（1）、その発見25年になる昨年までの引用件数は、ほぼ累積1万件を超えているようである［図1］。

我々は1986年に別記の固型腫瘍におけるEPR効果を発見したが、それ以前に細菌感染局所（炎症部）において細菌の産生するプロテアーゼが宿主のもつプロテアーゼ・カスケード［Hageman factor→kallikrein→kininogen→bradykinin(kinin)］を活性化し、血管作動物質キニンを生成することによって血管透過性亢進する（enhanced permeability→浮腫形成）ことを見出していた。これを検出するために青色色素エバンスブルーを静注すると、キニンの生成部位（プロテアーゼ投与部皮膚局所）でのみ青色色素と結合したアルブミンの漏出をみた［図2A］。これを固型癌に応用してみると、アルブミンなどの高分子の血清タンパクは選択的に腫瘍部でのみ漏出し、さらに正常の皮膚と違って、その腫瘍部で漏出・蓄積したタンパクは1～2週間後でもまだそこに保持（retention）されることを見出した。これをEPR効果（enhanced permeability and retention effect）と命名した（2）。

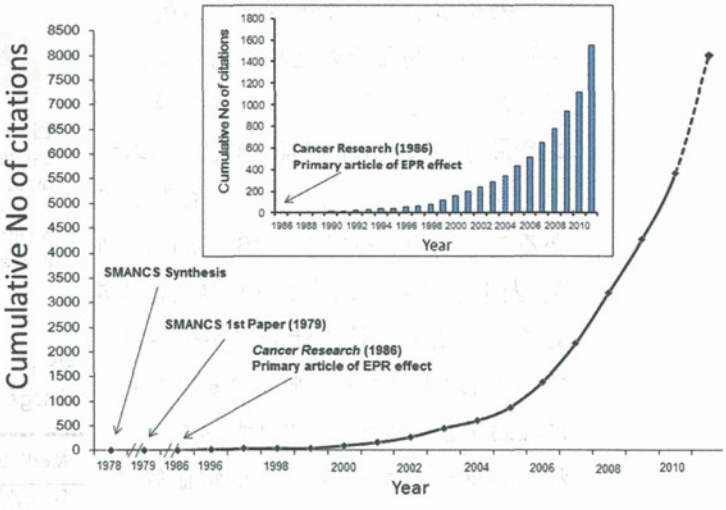

図1. Cumulative citation numbers of the EPR effect

これを生体親和性のある高分子HPMA（ヒドロキシプロピルメタアクリレートポリマー）で分子量を変えて調べてみると、血清タンパクと同じく、分子量約4万以上ではそのEPR効果を示したのである（3,4）。これら高分子の正常の炎症組織と癌組織での挙動の違いは、各々の局所での滞留性（時間）であるこ

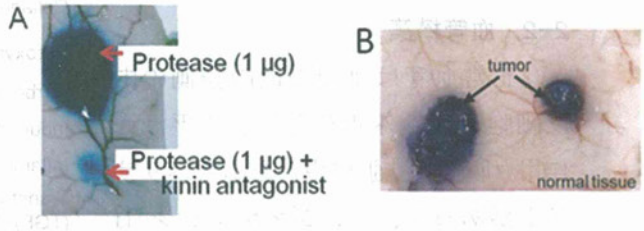

図2. A shows extravasation of an Evans blue-albumin complex induced by intradermal injection of serratial protease (top), however when a kinin antagonist in addition to the protease (bottom) were injected similarly, the extravasation was inhibited almost completely (ref. 6,7). B shows two tumor tissues exhibiting extravasation of the Evans blue-albumin complex only in tumor. No Evans blue-albumin leakage occurred in the normal skin seen in the background.

とがわかった（2〜3日 vs 数週、下記参照）。詳細は最近のレビューを参照されたい（3-7）。

2. EPR効果の要因

2-1. 血管作動物質

もともと癌形成（発癌）の早期では血管形成が盛んで、VEGFなどの細胞増生因子を癌細胞が分泌しているが、VEGFも内皮細胞の増殖促進作用の他に、血管透過性を高めている。我々はヒトおよび動物（マウス・ラット）で数多くの血管透過性増進因子を産出していることを明らかにしたが、そのなかでも上記のブラジキニン（8）、さらに一酸化窒素（誘導型NO合成酵素由来）は中心的なそのための血管作動因子である。その他にプロスタグランジンや最近では一酸化炭素（CO；ヘムオキシゲナーゼの作用による）も重要であることがわかってきた（6,7,9,11）[図3、表1]。これらは癌がマウスでは1.5gぐらいまでは特に活発に産生されて、それ以上になると腫瘍1g当たりになおすと減少する。注目すべきはそれらのメディエーターは正常血管にも作用することであり[図3]、正常組織に転移した癌細胞も正常血管からの栄養の摂取を容易にしている。

2-2. 血管構築

正常血管は血管の最内腔側の内皮細胞とその外側をとりまく平滑筋作用（収縮・拡張作用）を示すペリサイトがあって、アンジオテンシンII（AT-II）、NO、キニン、その他の血管作動因子で血管の内径が制御されるが、腫瘍血管では例えばAT-IIレセプターが欠損している、あるいはペリ

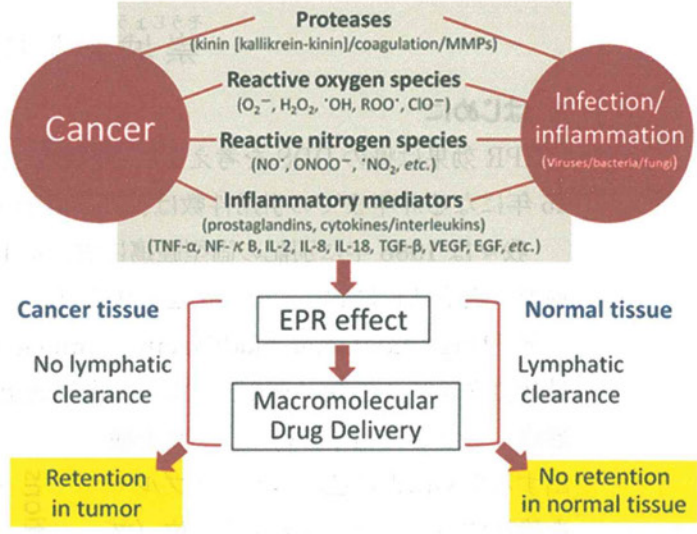

図3. Various vascular mediators commonly found in inflammation and cancer that contribute to the EPR effect. These mediators also affect normal blood vessels. A major difference between the two pathological phenomena is that the slower clearance rate of extravasated macromolecules, *i.e.* a prolonged retention time, in tumor tissue compared with that in inflamed tissues.

表1 Factors affecting the EPR effect of macromolecular drugs in solid tumors.[a]

Mediators	Responsible enzymes and mechanisms[b]
Bradykinin	Kallikrein/protease
NO	iNOS
VPF/VEGF	Involved in NO generation
Prostaglandins	Cyclooxygenase 1
Collagenase (MMPs)	Activated from proMMPs by peroxynitrite, or proteases
Peroxynitrite	$NO + O_2^{\cdot -}$
Carbon monoxide (CO)	Heme oxygenase (HO)-1
Induced hypertension	Using angiotensin II
Inflammatory cells and H_2O_2	Neutrophil/NADPH oxidase, etc
Transforming growth factor (TGF)-β inhibitor	
Tumor necrosis factor (TNF)-α	
Anticancer agents	
Heat	

[a]Extensive production of these vascular mediators that facilitate the extravasation from normal and tumor vessels. [b]The enzymes or mechanisms involved in each mediator are shown.

サイトを欠いているなど、構造上、機能上、著しい欠損があり、腫瘍血管の走行状態も、血流の流れも極めて不規則である。さらに、内皮細胞間の間隙も1～5μ大きく開いている場合もあるという。つまり、細菌（1～2μ）でさえも腫瘍部でより選択的に漏出するわけであり（5-7）、いわゆるリポゾームやミセル剤にとってはまことに透過しやすい状況である。従って、AT-IIで昇圧することによって、とくに腫瘍血管部を押し拡げてEPR効果を高めることができる（2～3倍）［図4］。実際の臨床で我々はAT-IIの静脈注入により全身血圧を昇圧状態になし、スマンクス/リピオドールを腫瘍栄養動脈内に注入するとデリバリーも上がり、薬効も大幅に改善することが可能になる。その結果はヒトの難治性の進行癌、例えば転移性肝癌、胆のう癌、腎癌、膵癌などの症例で証明されている（10）。

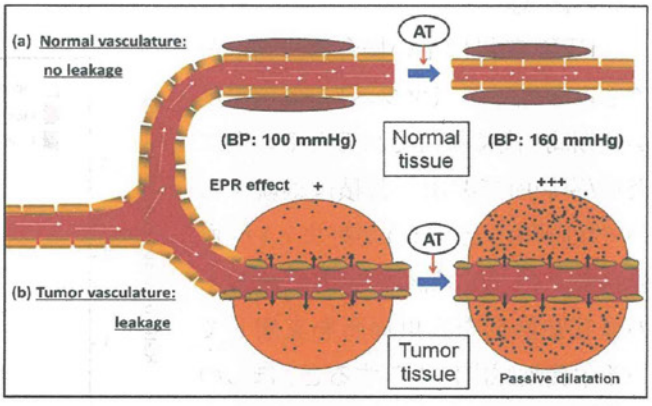

図4. Diagrammatic representation of the EPR effect and the effect of AT-II-induced hypertension accompanying the enhanced EPR effect and drug delivery in tumor tissue (b). Compare the effects in normal tissue (a). Under AT-II-induced hypertension (*e.g.* 100 → 160 mmHg), normal vessels and tumor vessels behaved differently. The normal blood vessels (a, right) have a smooth muscle cell layer that contracts and tightens the cell-cell junctions, and a narrowing of the vascular diameter that results in less drug leakage. In tumors (b), the vasculature endothelial cell-cell junctions open hydrodynamically (b, right). AT-II-induced hypertension thus leads to increased tumor-selective delivery of macromolecular drugs due to gap opening as demonstrated in clinical settings.

3. EPR効果の定義とその周辺の問題

上記のような状況から腎排泄のない高分子（分子量約4万以上）であれば何でもよいかというとそうではない。例えば変性タンパク質や高度に化学修飾をほどこした血清タンパク質（IgGなど）、あるいはα_2マクログロブリン（プロテアーゼ阻害タンパク）がプラスミン（プロテアーゼ）とE/I複合体になったものなどは、もともと数日もある血中半減期は5分～3hrほどに激減する［表2］。つまり、生体の異物認識機構により直ちに排除される。従って、これらを含めて生体親和性をEPR効果の第一のパラメータとして挙げることができる［表2～4］。表2、3に示すように、いわゆる生体親和性がある高分子であることがまず優先される。

これら分子量や生体親和性に加えて、表面電荷の問題がある。ナノ粒子（タンパク、リポゾーム、ミセル、遺伝子を含む超微粒子）などにおいて、例えば、塩基性の強いポリカチオンでは、静脈内投与後、数分で血中から消失する。酸性度の強いポリアニオン（例えば表面荷電－40mV）などは肝、ついで脾に効率的に蓄積し、数十分～数時間内に血中から消失する。一般に強い陽性荷電をもつポリマーは、血管内皮細胞表層におけるカルボキシレート基、サルフェート基などの負電荷が多く、強い陰性のため、血中半減期が極めて

短い［図 5］。

EPR 効果は早い場合には約十分でもみられるが（マウス）、血中濃度が長期間、高く維持されるとその間に炎症/癌局所で漏出・蓄積は継続するので数時間以上のほうが好ましい。血管造影というX線診断法では、低分子の血管造影剤を病巣局所を支配している栄養動脈内に投与すると、ほんの一過性（1～2 分以内）には腫瘍部で漏出し、X線画像上には腫瘍が濃染して見えるが、水溶性・低分子の造影剤は自由拡散により、急速に消失する。これはいわゆる passive targeting である。これに対し、EPR では例えばリピオドール（油性造影剤）の動注では腫瘍部のみに何週（～数ヶ月）も滞留する。この間、スマンクスのように薬剤が徐放すれば効果（毒力）は癌部のみで持続し、副作用のない治療が可能となる（5,7,10）。

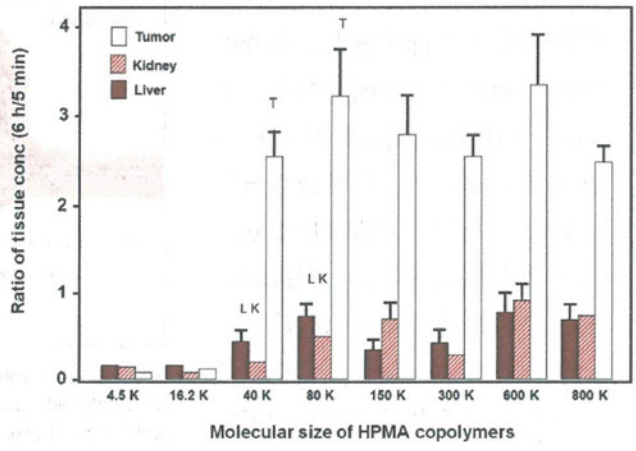

図 5. Tumoritropic uptake of the biocompatible macromolecule *N*-(2-hydroxypropyl)methacrylamide (HPMA) polymer containing radioactive ^{131}I-labeled tyrosine. The EPR effect leading to higher uptake of the HPMA polymer into tumors is seen for polymer sizes larger than 40 kDa. The amount of uptake at 6 h is compared with that at 5 min. That is, tumor uptake increases with time.

表 2 Characteristics needed for the EPR effect of nanomedicines and macromolecular drugs.

Biocompatibility	No interaction with blood components or blood vessels, no antigenicity, no clearance by the reticuloendothelial system, no cell lysis. Biologically inert.
Molecular size	Larger than 40 kDa (larger than the renal clearance threshold).
Surface charge	Weakly negative to near neutral.
Time required to achieve	Longer than several hours in systemic circulation in mice, with distinct accumulation seen at 30 min.
Drug retention time	Usually days to weeks, in great contrast to passive targeting, in which low-molecular-weight contrast imaging agents are rapidly accumulate in tumor, but cleared by diffusion into the systemic circulation in a few minutes.

[a] Compare with low-molecular-weight contrast agents in angiography, which is taken up in the tumor tissue by passive targeting, but not retained. Arterial injection of low molecular weight anticancer agents, though they hit tumor by the first path effect, is not retained in tumor tissue, and so not much benefit clinically.

表 3　Plasma clearance times of selected modified and native proteins *in vivo*.[a]

Proteins	Species difference, original/test	Probe modification	pI	MW (kDa)	$t_{1/2}$
Albumin	Mouse/mouse	None	4.8	68	72–96 h
	Mouse/mouse	DTPA (^{51}Cr)	≤4.8	—	6 h
	Cow/mouse	DTPA (^{51}Cr)	≤4.8	—	1 h
Formaldehyde-modified albumin	Human/rat	^{125}I-labeled formaldehyde	≤4.8	—	25 min
α_2-Macroglobulin	Human/mouse	^{125}I	5.3	180×4	140 h
α_2-Macroglobulin-plasmin complex	Human/mouse	^{125}I	—	180×4	5 min
Interferon (IFN-α)	Human/human	None	—	18	8 h (sc)
PEG-IFN-α2a	Human/human	PEG	—	52	80 h (sc)

[a]DTPA, diethylenetriaminepentaacetic acid; IFN, interferon; PEG, polyethylene glycol; sc, given subcutaneously. (Data modified from ref. 12 (a) and (b))

表　4　Surface charge affecting plasma residence times of different nanoparticles in mice.

Type of nanoparticles	ζ potential (mV)	Mean particle size (nm)	Plasma residence time		Remarks
			$T_{1/2}$	$T_{1/10}$	
Liposome					
Non-PEGylated	-7.31	124	9.08 h	>24 h	Doxorubicin loaded, DPPC:Chol = 1:1
Weakly cationic	+5.58	131	4.51 h	15 h (mean)	Doxorubicin loaded, DPPC:Chol:DC-Chol = 5:4:1, slightly positive
Strongly cationic	+24.25	95	<30 min	<10 min	Doxorubicin loaded, DPPC:DC-Chol = 5:5, strongly positive
Poly-L-Lys/DNA	Positive	—	<5 min	30 min	^{32}P-labeled 8-kbp DNA
Chitosan nanoparticle					
Weakly anionic	-13.2	149.2	—	12 h (mean)	CM/MM = 1:2, slightly negative
Strongly anionic	-38.4	156.0	—	3 h (mean)	CM/MM = 2:1, strongly negative
Weakly cationic	+14.8	150.1	—	<1 h	CH/MM = 1:1, slightly positive
Strongly cationic	+34.6	152.7	—	<1 h	CH/MM = 2:1, strongly positive

DPPC, dipalmitoylphosphatidylcholine; Chol, cholesterol; CM, carboxymethyl chitosan; MM: methyl methacrylate polymer.　(Data modified from ref. 13)

5. EPR 効果と蛍光ナノプローブによる腫瘍の蛍光イメージングと PDT（光照射療法）

当初、我々は EPR 効果を肉眼的にエバンスブルーアルブミンによる腫瘍部の選択的に濃染像として確認し、さらにより普遍的に合成高分子で生体親和性の極めて高い HPMA（ヒドロキシプロピルメタアクリルレート）ポリマーにチロシンを導入し、その放射性ヨード化物を用いてより放射能のカウントにより系統的に数値化してその詳細をみた（2,3,4）。

最近、同じことをローダミンイソチオシアネート（RITC）標識アルブミンを用いて担癌（S-180）マウスの系で検討したところ、フリーの低分子ローダミン B（MW479.1）では全く腫瘍集積性がないのに対し、RITC-BSA（分子量約 7 万）は鮮明な腫瘍の蛍光像を呈した。蛍光画像イメージング装置 IVIS により、正常部よりも腫瘍部は 10 倍以上の蛍光を発していた。我々はこれを内視鏡装置に応用し、内視鏡による蛍光検出を施行することに

よって、超早期癌の検出を目指した研究を展開している。

一般に、光照射療法は He/Ne レーザー光線（出力波長 635nm）により励起した蛍光プローブから、一重項酸素を発し、殺細胞作用になるが、今回、内視鏡のキセノン光源でも 2～3cm 以上の深度に充分な組織透過性を示し、HPMA-ZnPP の場合、光照射によってはじめて著明な抗腫瘍効果がみとめられた。この場合、EPR 効果による蛍光増感ナノプローブの腫瘍選択的集積を可能にし、その蛍光部（腫瘍部）のみの可視光の照射でその局所のみのピンポイントな治療ができるという点で、将来、管腔臓器（例えば口腔、食道、胃、腸、膀胱、子宮、腹腔、胸腔、気管支、尿道など、および肉腫や皮膚癌などの表層癌）等への広範な応用が期待される。これはまた、従来の低分子蛍光増感プローブが全身に分布し。日常の明るさでも皮膚に障害を与えるのに対し、この HPMA-ZnPP では腫瘍選択性が高いので、皮膚障害はみられない。

6. 結び

EPR 効果発見 26 年になるが、スマンクス以外に近年、ようやくリポゾーム製剤、ミセル製剤、抗体薬などの高分子制癌剤の第一世代のプロトタイプ型抗癌剤が認識されてきた。ここ 10-20 年の間に、活性本体の release 制御（pH、プロテアーゼ sensitive により可能）、血中動態（長い $t_{1/2}$）、癌組織内の浸透性等の個々の問題点が理解されるようになり、図 6 に示す各ステップに対し、夫々の方策が明らかとなってきた。いよいよこれからが高分子型製剤の出番である。蛍光イメージングはまさに EPR 効果の証明そのものであり、上記の ZnPP ポリマー製剤は今後、蛍光内視鏡を用いたいわゆる Theranostics のさきがけとなることを願っている。このようなナノプローブによる早期発見とその PDT による早期治療は、まさにその一石二鳥を可能にしようとするものである。

Steps	Barriers to be overcome	Comments
1st	**Vascular wall**/Circulating Blood **EPR effect**/Extravasation into tumor tissue ↓ Tumor tissue/interstitial space	Polymeric drugs/nanomedicines Vascular wall openings Enhancement of the EPR effect by NO and angiotensin-converting enzyme inhibitor
2nd	Dissemination to tumor cells ↓	Stromal matrix/fibrin gel/fibroblast: protease/plasmin/plasminogen activator
3rd	Cell membrane/**internalization** ↓	**Endocytic uptake** **Styrene-co-maleic acid (SMA) micelle disintegration**
4th	**Drug release**/free active drug pH/protease-labile linker Interact with target molecules ↓	No reverse exocytosis Hydrazone/maleic acid
5th	**In vivo antitumor effect: 100% survival/cure** ↓	React with target molecules High antitumor efficacy *in vivo*
6th	**Regulatory steps/safety issue** ↓	Phase I, II, III trials
7th	**Cost/benefit**	More universal tumor targets [Evaluation by Natl. Inst. Health Clin. Excellence, UK]

図6. Barriers to the development of macromolecular drugs for cancer and steps to be overcome.

8．参考文献

(1) V. Torchilin, Tumor delivery of macromolecular drugs based on the EPR effect, Adv. Drug Deliv. Rev. 63, 131-135 (2011).

(2) Y. Matsumura and H. Maeda: A new concept for macromolecular therapeutics in cancer chemotherapy: Mechanism of tumoritropic accumulation of proteins and the antitumor agent SMANCS. **Cancer Res.**, 46, 6387-6392 (1986)

(3) Y. Noguchi, J. Wu, R. Duncan, J. Strohalm, K. Ulbrich, T. Akaike and H. Maeda: Early phase tumor accumulation of macromolecules: A great difference in clearance rate between tumor and normal tissues. **Jpn. J. Cancer Res.**, 89, 307-314 (1998)

(4) H. Maeda, J. Wu, T. Sawa, Y. Matsumura and K. Hori: [Review] Tumor vascular permeability and the EPR effect in macromolecular therapeutics. **J. Cont. Release**, 65, 271-284 (2000)

(5) H. Maeda, T. Sawa, and T. Konno: Mechanism of tumor-targeted deliverly of macromolecular drugs, including the EPR effect in solid tumor and clinical overview of the prototype polymeric drug SMANCS. **J. Cont. Release,** 74, 47-61 (2001)

(6) H. Maeda: Tumor-selective delivery of macromolecular drugs via the EPR effect: Background and future prospects, **Bioconj. Chem**. 21, 797-802 (2010)

(7) H. Maeda: Vascular permeability in cancer and infection as related to macromolecular drug delivery, with emphasis on the EPR effect for tumor-selective drug targeting. **Proc. Jpn. Academy, Series B**. 88, 53-71 (2012)

(8) H. Maeda, Y. Matsumura and H. Kato: Purification and identification of [hydroxyprolyl3] bradykinin in ascitic fluid from a patient with gastric cancer. **J. Biol Chem.**, 263, 16051-16054 (1988)

(9) H. Maeda, Y. Noguchi, K. Sato and T. Akaike: Enhanced vascular permeability in solid tumor is mediated by nitric oxide and inhibited by both new nitric oxide scavenger and nitric oxide synthase inhibitor. **Jpn. J. Cancer Res**., 85, 331-334 (1994)

(10) A. Nagamitsu, K. Greish, H. Maeda, Elevating blood pressure as a strategy to increase tumor targeted delivery of macromolecular drug SMANCS: Cases of advanced solid tumors, **Japan. J. Clinical Oncol.** 39, **756-766** (2009)

(11) J. Wu, T. Akaike and H. Maeda: Modulation of enhanced vascular permeability in tumors by a bradykinin antagonist, a cyclooxygenase inhibitor, and a nitric oxide scavenger. **Cancer Res.**, 58, 159-165 (1998)

(12) (a) H. Maeda, Y. Matsumura, T. Oda and K. Sasamoto: Cancer selective macromolecular therapeutics: Tailoring of an antitumor protein drug. *In* **Protein Tailoring for Food and Medical Uses** (eds: R.E. Feeney and J.R. Whitaker), Marcel Dekker, Inc., New York-Basel, p. 353-382 (1986)

(b) K. Greish, J. Fang, T. Inuzuka, A. Nagamitsu and H. Maeda: Macromolecular anticancer therapeutics for effective solid tumor targeting: Advantages and prospects. **Clinical Pharmacokinetics**, 42, 1089-1105 (2003)

(13) C. He, Y. Hu, L. Yin, C. Tang, and C. Yin, Effects of particle size and surface charge on cellular uptake and biodistribution of polymeric nanoparticles," *Biomaterials*, 31, 3657–3666 (2010).

Tumor targeting polymeric drugS based on the EPR effect; Its augmentation for drug delivery and efficacy, and extention to tumor imaging

Hiroshi Maeda

Research Institute of Drug Delivery System, Sojo University

Ever since the beginning of cancer chemotherapy, the major problem has been severe toxicity of anticancer drugs; the first reason for this matter is that toxic anticancer drugs affect both normal cells and tumor cells similarly. Second reason is that these drugs will be distributed either tumor or normal tissue indiscriminately.

We realized that solid tumor has quite different blood vessels anatomically and pathologically. When the biocompatible macromolecules are injected intravenously, they leak out much more into the tumor; i.e. vascular permeability is enhanced in tumor. Furthermore, the macromolecules thus extravasated into the tumor will be retained there for a long time (to weeks). This phenomenon was coined "the enhanced permeability and retention (EPR) effect" of macromolecules, which is applicable to the molecular size > 40 KDa.

In diversified tumors in vivo, however, they exhibit heterogeneity in the EPR effect that would result in inconsistent tumor drug delivery, and result in therapeutic failure. We now found ways to overcome this heterogeneity of EPR effect by using NO releasing agents (eg. nitroglycerin), angiotensin converting enzyme inhibitor, angiotensin II induced hypertension and others.

Thus, EPR effect based nanomedicine for cancer would offer us the first rational ways to the development of tumor targeted drugs. This will not only provides better therapeutic opinion, but also can be extend to the tumor imaging using fluorescent nanoprobes for selective visualization of tumor. We now developed fluorescent nanoprobes for endoscopic tumor detection about which we will report in this meeting. These nanoprobes can be changed to generate singlet oxygen [$^1O_2$] upon light irradiation. Consequently, one can achieve detection and treatment simultaneously by [$^1O_2$] as cytotoxic principle thus generated only at the tumor site.

<Reference> H. Maeda, *Proc. Jpn. Academy, Series B.* 88, 53-71 (2012)

Journal of Controlled Release 165 (2013) 191–198

Contents lists available at SciVerse ScienceDirect

Journal of Controlled Release

journal homepage: www.elsevier.com/locate/jconrel

Micelles of zinc protoporphyrin conjugated to *N*-(2-hydroxypropyl)methacrylamide (HPMA) copolymer for imaging and light-induced antitumor effects in vivo

Hideaki Nakamura [a,b], Long Liao [a], Yuki Hitaka [a], Kenji Tsukigawa [a], Vladimir Subr [c], Jun Fang [a,b], Karel Ulbrich [c], Hiroshi Maeda [a,*]

[a] Research Institute for Drug Delivery System, Faculty of Pharmaceutical Science, Sojo University, Kumamoto, Japan
[b] Laboratory of Microbiology and Oncology, Faculty of Pharmaceutical Science, Sojo University, Kumamoto, Japan
[c] Institute of Macromolecular Chemistry, Academy of Sciences of the Czech Republic, Prague, Czech Republic

ARTICLE INFO

Article history:
Received 19 September 2012
Accepted 25 November 2012
Available online 3 December 2012

Keywords:
Fluorescence imaging
Fluorescent nanoprobe
Singlet oxygen
Tumor targeting
HPMA-ZnPP conjugate
EPR effect

ABSTRACT

We synthesized *N*-(2-hydroxypropyl)methacrylamide polymer conjugated with zinc protoporphyrin (HPMA-ZnPP) and evaluated its application for tumor detection by imaging and treatment by light exposure using in mouse sarcoma model. To characterize HPMA-ZnPP micelle, we measured its micellar size, surface charge, stability, photochemical, biochemical properties and tissue distribution. In vivo anti-tumor effect and fluorescence imaging were carried out to validate the tumor selective accumulation and therapeutic effect by inducing singlet oxygen by light exposure. HPMA-ZnPP was highly water soluble and formed micelles spontaneously having hydrophobic clustered head group of ZnPP, in aqueous solution, with a hydrodynamic diameter of 82.8 ± 41.8 nm and zeta-potential of + 1.12 mV. HPMA-ZnPP had a long plasma half-life and effectively and selectively accumulated in tumors. Although HPMA-ZnPP alone had no toxicity in S-180 tumor-bearing mice, light-irradiation significantly suppressed tumor growth in vivo, similar to the cytotoxicity to HeLa cells in vitro upon endoscopic light-irradiation. HPMA-ZnPP can visualize tumors by fluorescence after i.v. injection, which suggests that this micelle may be useful for both tumor imaging and therapy. Here we describe preparation of a new fluorescence nanoprobe that is useful for simultaneous tumor imaging and treatment, and application to fluorescence endoscopy is now at visible distance.

1. Introduction

Photodynamic therapy (PDT) employs a photosensitizer and cytotoxic light-induced singlet oxygen ($^1O_2$) generation. $^1O_2$ generation damages DNA, RNA, proteins and lipids, which leads to cell death. Porphyrin derivatives usually generate cytotoxic $^1O_2$ after light irradiation that corresponds to the absorption wavelength of porphyrin derivatives [1–3]. Laserphyrin® and Photofrin® and others are well known porphyrin derivatives that are approved for limited use in conventional clinical PDT for early-stage lung (bronchogenic) or superficial cancer accessible to exciting light (laser irradiation at 630 nm) [4,5]. However, small molecular photosensitizers are expected to be distributed throughout the body including skin and other organs, and most have limited tumor selectivity or tumor-imaging capacity. Thus, they would cause cutaneous hyper-photosensitivity as the major adverse effect, which limits therapeutic success.

To solve this problem, one can utilize macromolecular photosensitizers, which have much longer half-lives in circulation and gradually and selectively accumulate in tumor tissues because of the EPR (enhanced permeability and retention) effect, accompanying much less accumulation in normal tissue [6–11]. Our group previously reported that biocompatible macromolecules (MW > 40 kDa) showed the EPR effect and accumulated selectively in tumors [6,12,13]. For the EPR effect to operate, the macromolecular surface charge is as important a determinant as is molecular size; a neutral to slightly negative charge and MW of > 40 kDa are preferable for tumor targeting [6,12,14]. In this study, we utilized a conjugate of zinc protoporphyrin (ZnPP) and 12-kDa *N*-(2-hydroxypropyl)methacrylamide (HPMA) copolymer, which has a neutral charge and is highly biocompatible. The conjugate behaved as a large macromolecule (apparent MW is 198-kDa), as do many polymer conjugates of low-molecular-weight micellar drugs that show preferential tumor accumulation [15–18].

Light-irradiated (at 420 nm, absorption max of ZnPP) ZnPP effectively generates $^1O_2$ and thereby exhibits potent cytotoxicity [18,19]. ZnPP is also a potent inhibitor of heme oxygenase-1 (HO-1), or HSP-32, which is a survival factor. HO-1 is highly upregulated in many cancer tissues in vivo and confers an antioxidative function to cells. Therefore, inhibition of HO-1 by ZnPP makes tumor cells more vulnerable to oxystress, the result being selective tumor regression. Most of normal cells are not affected because HO-1 in normal cells is expressed only at low level and insignificant. However, ZnPP is highly hydrophobic and soluble only in alkaline solutions or organic solvents. This

* Corresponding author at: Institute for DDS, Sojo University, Ikeda 4-22-1, Kumamoto, 860-0082, Japan. Tel.: +81 96 326 4114; fax: +81 96 326 3185.
E-mail address: hirmaeda@ph.sojo-u.ac.jp (H. Maeda).

0168-3659/$ – see front matter © 2012 Elsevier B.V. All rights reserved.
http://dx.doi.org/10.1016/j.jconrel.2012.11.017

insolubility of ZnPP in physiological aqueous solution hampers its therapeutic application. To overcome this obstacle, we developed water-soluble ZnPP micelles: one is styrene maleic acid copolymer (SMA) micelles that encapsulate ZnPP and forms nanomicelles (SMA-ZnPP), the other is pegylated ZnPP (PEG-ZnPP) [18–22]. Both ZnPP micelles alone exhibited antitumor activity, and light irradiation greatly enhanced this activity [18]. Despite high tumor accumulation of PEG-ZnPP and significant antitumor activity, the maximum ZnPP loading in PEG-ZnPP is theoretically about 6% (wt/wt), so the intravenous (i.v.) dose of PEG-ZnPP may become several grams to achieve therapeutic concentrations. Although ZnPP loading of SMA-ZnPP can be increased to about 50%, SMA-ZnPP micelles tended to accumulate predominantly in the liver and spleen [23]. Therefore, we aimed to develop another type of ZnPP micelles with greater tumor targeting and adequate loading of ZnPP.

Here, we describe the synthesis of HPMA-ZnPP, which spontaneously formed micelles in aqueous solution. We examined its size distribution, spectroscopic property, micelle stability, generation of $^1O_2$, cellular uptake, tumor and tissue distribution and antitumor activity in vivo when used with xenon light-irradiation. Other important results concern simultaneous in vivo fluorescence imaging of the whole animal from outside, and the therapeutic effect of the polymer-photosensitizer conjugate.

2. Materials and methods

2.1. Materials

Male ddY mice were purchased from Kyudo Co., Ltd, Saga, Japan. Protoporphyrin IX, zinc acetate, triethylamine, dimethylaminopyridine, diethylether, Tween 20 and egg lecithin of reagent grade were purchased from Wako Pure Chemical, Osaka, Japan. 1-Ethyl-3-(3-dimethylaminopropyl)carbodiimide and 3-(4,5-dimethyl-2-thiazolyl)-2,5-diphenyl-2H-tetrazolium bromide (MTT) were purchased from Dojindo Chemical Laboratory, Kumamoto, Japan. 2,2,6,6-Tetramethyl-4-piperidone (4-oxo-TEMP) was purchased from Tokyo Chemical Industry, Tokyo, Japan. The HPMA polymer (mean MW ~12 kDa) we used contains one free amino group at the end, and was prepared at the Institute of Macromolecular Chemistry, Prague, Czech Republic.

2.2. Synthesis of HPMA-ZnPP

Scheme 1 shows the synthesis of HPMA-ZnPP conjugate, in which conjugation of carboxyl group of free ZnPP with either hydroxyl group or amino group of HPMA (mean MW 12 kDa) was carried out to form ester and amide bonds, respectively. In brief, 570 mg of HPMA as Scheme 1 and 281 mg of ZnPP were mixed in 50 ml of DMSO at 50 °C and reacted by addition of 1.0 g of triethylamine, 1.2 g of dimethylaminopyridine and 1.9 g of 1-ethyl-3-(3-dimethylaminopropyl)carbodiimide hydrochloride as a catalyst for 12 h at 50 °C in the dark. After the reaction, HPMA-ZnPP conjugates were precipitated by addition of diethylether (200 ml), and reaction catalyst in the supernatant was removed by centrifugation. The conjugates were washed three times with diethylether to remove the reaction catalyst and DMSO. HPMA-ZnPP was purified via gel permeation chromatography (Bio-Beads SX-1, BioRad, Hercules, CA) using dimethylformamide (DMF) as elute. Peak fraction of elutes was ultrafiltrated with membrane filter with a cutoff molecular size of 100 kDa, to remove decomposed or unreacted small molecules and to replace the DMF to distilled water. Fluffy powder (635 mg) was obtained by lyophilization.

2.3. Gel permeation column chromatography

Analytical gel permeation column chromatography of HPMA-ZnPP was performed with Bio-Beads SX-1 using a column ($\varphi = 2.5$ cm, $L = 60$ cm) and eluted with DMF at a flow rate of 0.1 ml/min. 1.5 ml fractions of elutes were measured at absorbance at 422 nm, which corresponded to ZnPP absorbance.

2.4. Fluorescence spectroscopy and fluorescence polarization

HPMA-ZnPP at 10 μg/ml was dissolved in PBS containing Tween 20 (0.0005–0.5%) or urea (1–9 M), and fluorescence spectra were measured with a fluorescence spectrophotometer (FP-6600; JASCO, Tokyo). HPMA-ZnPP (2.5 μg/ml) or free ZnPP (0.5 μg/ml) was dissolved in DMF, and sample solutions were then excited at 420 nm by a fixed polarized light; fluorescence emission at 590 nm was recorded at parallel (0°) and perpendicular (90°) angles of the secondary polarizer, which was equipped in a Model FP-6600 fluorescence spectrophotometer. The fluorescence polarization value (P value) was calculated by using the equation $P = (I_{//} - I_{\perp})/(I_{//} + I_{\perp})$, where $I_{//}$ = fluorescence intensity of the parallel component and $I_{\perp}$ = fluorescence intensity of the perpendicular component. The fluorescent polarization value is proportional to the molecular size of the fluorescent probe [24].

2.5. High performance liquid chromatography (HPLC)

Cleavage of ester bond of this conjugate HPMA-ZnPP was analyzed by using HPLC (Prominence, Shimadzu, Kyoto, Japan) with the multimode size exclusion column GF-310 HQ (300×7.5 mm) with photodiode array detection at 422 nm, which was eluted with a mixture of 30% DMSO and 70% methanol containing 10 ppm trifluoroacetic acid at 1.0 ml/min.

2.6. Dynamic light scattering and zeta potential

HPMA-ZnPP or HPMA was dissolved in 0.01 M phosphate-buffered 0.15 M saline (PBS, pH 7.4) at 1 mg/ml and was filtered through a 0.2 μm filter attached to a syringe. The particle size and surface charge (zeta potential) were measured by light scattering (ELS-Z2; Otsuka Photal Electronics Co. Ltd., Osaka).

2.7. Transmission electron microscopy (TEM)

A drop of HPMA-ZnPP (0.1 mg/ml) was applied to a copper grid coated with carbon film and air-dried. The micelle image and size of

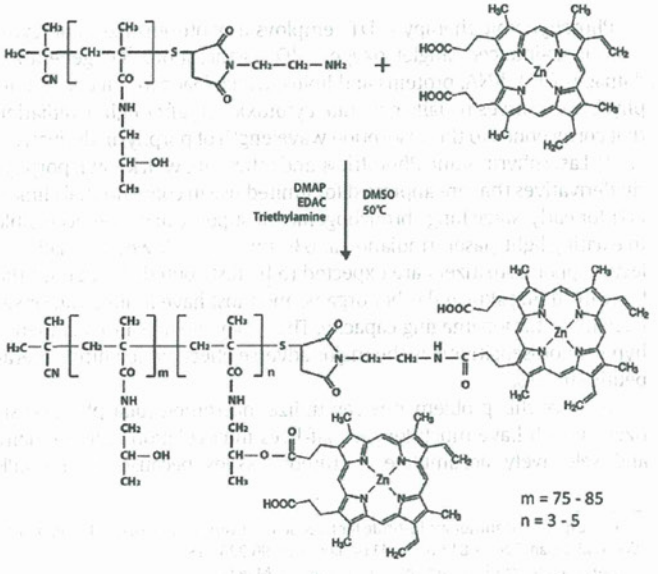

Scheme 1. HPMA-ZnPP synthesis. Chemical structures and conjugation pathway. ZnPP was conjugated to the secondary hydroxyl group and the terminal amino group of HPMA.

HPMA-ZnPP were analyzed by using a transmission electron microscope (Tecnai F20; FEI, Hillsboro, OR).

2.8. Electron spin resonance (ESR) spectroscopy

ESR spectra were measured by using an ESR spectrometer at 25 °C (JES FA-100; JEOL, Tokyo). Sample solutions containing 200 μg/ml HPMA-ZnPP (or 40 μg/ml ZnPP) and 20 mM 4-oxo-TEMP with or without light irradiation were evaluated. Samples in a flat quartz cell (Labotec, Tokyo) were irradiated (28 mW/cm^2) by using xenon light at 400–800 nm (MAX-303; Asahi Spectra, Tokyo) for indicated times. The ESR spectrometer was usually set at a microwave power of 1.0 mW, amplitude of 100-kHz and field modulation width of 0.1 mT.

2.9. Cytotoxicity assay

HeLa cells were maintained in DMEM supplemented with 10% fetal calf serum under 5% CO_2/air at 37 °C. HPMA-ZnPP or ZnPP was added 24 h after plating HeLa cells at 3000 per well in 96-well plates. Irradiation with fluorescent blue light having peak emission at 420 nm (TL-D; Philips, Eindhoven, Netherland) with 1.0 J/cm^2 per 15 min was then performed. After 48 h of culture, the MTT assay was carried out to quantify viable cells, with absorbance at 570 nm as described by instruction of the manufacture.

2.10. Intracellular uptake

HPMA-ZnPP or free ZnPP was added at a concentration of 20 μg ZnPP equivalent/ml 48 h after plating HeLa cells at 25,000 cells per well in 24-well plates (1.9 cm^2/well). At indicated time periods, cells were washed with PBS and added with 2 ml ethanol followed by sonication (20 W, 30 s) to extract the HPMA-ZnPP or free ZnPP. Concentration of ZnPP was measured by fluorescence intensity (Ex. 422 nm, Em. 590 nm).

2.11. In vivo antitumor activity

The care and maintenance of animals were undertaken in accordance with the institutional guidelines of the Institutional Animal Care and Use Committee of Sojo University. Mouse sarcoma S-180 cells (2×10^6 cells) were implanted s.c. in the dorsal skin of ddY mice. When tumor reached to diameter of about 5 mm, 15 mg/kg of ZnPP equivalent drugs in saline was injected i.v. Then after 24, 48 and 72 h, tumor was irradiated by xenon light (MAX-303; Asahi Spectra) at 400–800 nm (20 mW/cm^2) for 5 min as described. Tumor volume (mm^3) was calculated as $(W^2\times L)/2$ by measuring the length (L) and width (W) of the tumor on the dorsal skin.

2.12. Pharmacokinetics and tissue distribution of HPMA-ZnPP

When S-180 tumor in mice with tumor diameter of approximately 10 mm, injected i.v. was 15 mg of ZnPP equivalent per kg of free ZnPP or HPMA-ZnPP. At the indicated times, mice were killed, perfused with physiological saline and dissected, and then tissues were weighed, DMSO (1 ml per 100 mg of tissue) was added, and samples were homogenized and centrifuged (12,000 g, 25 °C, 10 min) to precipitate insoluble tissue debris, and ZnPP and HPMA-ZnPP in the supernatant were quantified by fluorescence intensity (excitation at 422 nm, emission at 590 nm).

2.13. In vivo fluorescence imaging

Tumor-bearing mice as described above were injected with 15 mg of ZnPP (equivalent) per kg i.v. At 24 h after injection, mice were shaved and, under isoflurane gas anesthesia, were subjected to in vivo fluorescence imaging using IVIS XR (Caliper Life Science, Hopkinton, MA) (excitation at 430 ± 15 nm and emission at 695–770 nm). Fluorescent images of each tissue were also observed after dissection.

3. Results

3.1. Synthesis of HPMA-ZnPP

The carboxyl group of ZnPP was conjugated to HPMA at the secondary hydroxyl group and the terminal amino group (Scheme 1). Gel permeation chromatography of the reaction product on Bio-beads column showed that HPMA-ZnPP had a higher molecular weight than free ZnPP, and neither free ZnPP nor decomposition product was detected (Fig. 1A). The total yield was 47% (wt/wt) based on ZnPP. The macromolecular characteristics of HPMA-ZnPP were also examined by fluorescence polarization. The polarization value (P value) of free ZnPP in dimethylformamide (DMF) was 0.0064, whereas that of HPMA-ZnPP was 0.0378, which suggests that HPMA-ZnPP had a higher molecular weight than ZnPP (Fig. 1B). Also HPMA-ZnPP was shown to have good water solubility of more than 30 mg/ml in water. The ZnPP content in HPMA-ZnPP was estimated as 20% (wt/wt) on the basis of absorbance of ZnPP.

3.2. Micellar structure of HPMA-ZnPP

ZnPP is highly hydrophobic and is believed to form aggregates in water by π–π stacking interactions between tetrapyrrole planes. Thus, we anticipated that HPMA-ZnPP would form micellar structures in aqueous solution; namely ZnPP containing head group can form a hydrophobic inner core as clustered head group, and a hydrophilic HPMA chain as tail would form an outer surface layer facing toward water. Fig. 1C shows that either amide or ester bonds between HPMA and ZnPP are stable in DMSO and in alkaline pH (10 mM NaOH) without DMSO, separately. However, alkaline treatment in DMSO efficiently cleaved HPMA-ZnPP since the micellar structure is disintegrated in organic solvent (DMSO), and OH− becomes accessible to ester bond and resulted in hydrolyzes of ester bond and release of free ZnPP. Dynamic light scattering analyses showed that in aqueous solution of HPMA-ZnPP it formed large micelles particles (hydrodynamic diameter: 82.8 ± 41.8 nm), which suggests that HPMA-ZnPP was associated into micelles in aqueous solution, whereas HPMA alone had a hydrodynamic diameter of 5.6 ± 1.9 nm (Fig. 1D). Transmission electron microscopy also showed the micelle size of HPMA-ZnPP as 30–80 nm (Fig. 1E). HPMA-ZnPP micelles in phosphate-buffered saline (PBS) showed almost neutral zeta potential (+1.12 mV).

3.3. HPMA-ZnPP formed micelles via hydrophobic interaction

ZnPP has a λ_{max} at 422 nm in organic solvents such as DMSO and ethanol, and it exists as monodispersed free molecules. However, when free ZnPP molecules aggregate with each other in soluble form in aqueous solution, the λ_{max} shifts towards a shorter wavelength (390 nm). This blue shift was also observed when HPMA-ZnPP was dissolved in aqueous solution (Fig. 1F). Furthermore, the blue shift decreased after adding detergent or Tween 20, or when dissolved in DMSO, but not in the presence of 9 M urea (Fig. 1F). Measurement of fluorescence intensity of HPMA-ZnPP revealed the same phenomenon; HPMA-ZnPP fluorescence was quenched in aqueous solution, which indicates a hydrophobic interaction among aromatic rings or π–π stacking of ZnPP, whereas HPMA-ZnPP fluorescence intensity was restored by adding detergent but not 9 M urea (Fig. 1G, H).

3.4. Demonstration of $^1O_2$ generation from HPMA-ZnPP

The $^1O_2$-generating capacity of HPMA-ZnPP was examined by means of ESR spectroscopy with the use of spin-trapping agent

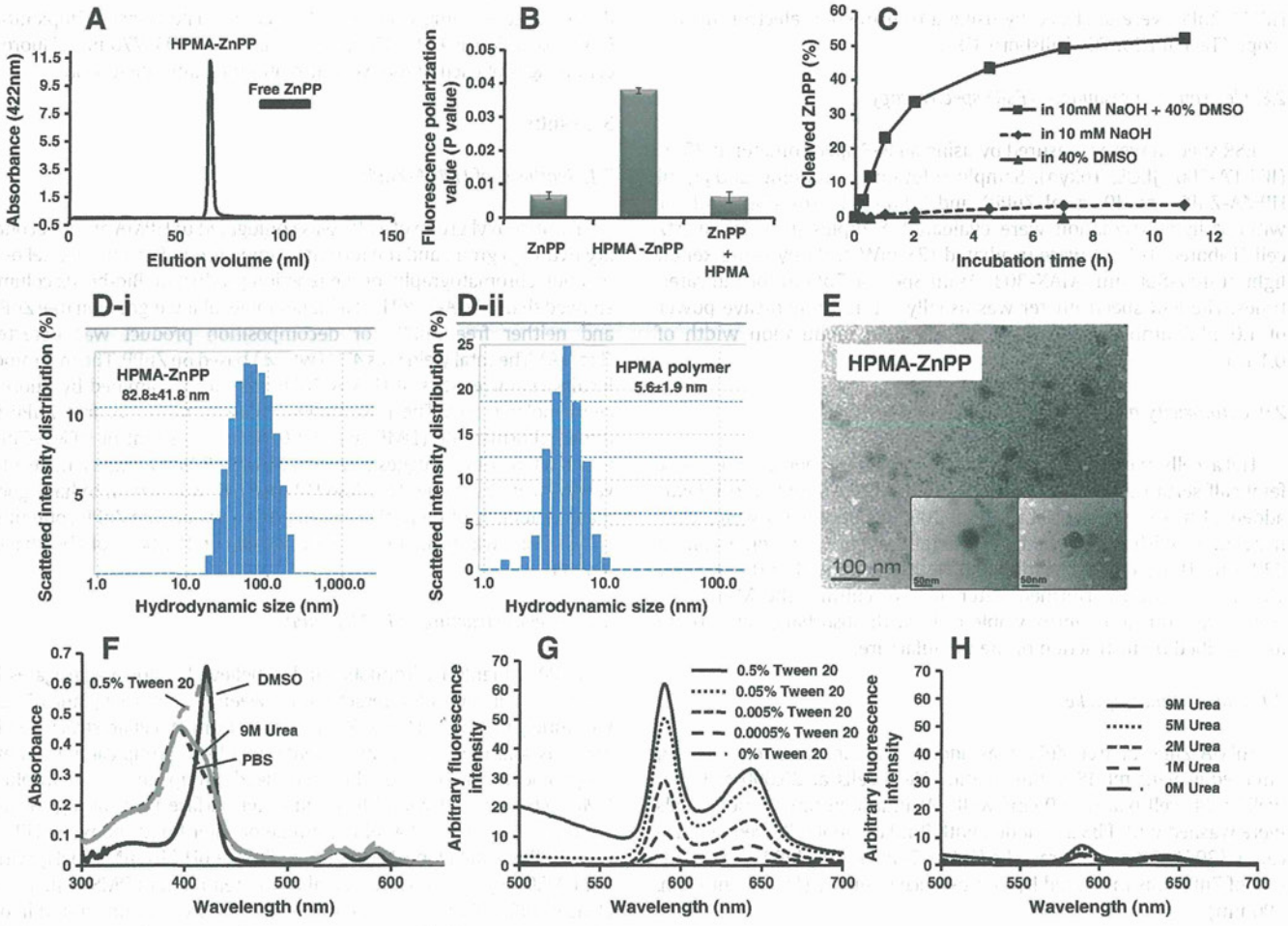

Fig. 1. Properties of HPMA-ZnPP in an organic solvent and aqueous solution. (A) HPMA-ZnPP at 1 or 0.2 mg/ml ZnPP was applied to a Bio-Beads S-X1 column and eluted by DMF, and detected by absorption at 422 nm. The dark bar shows the position of elution of free ZnPP. (B) Fluorescence polarization of ZnPP at 0.5 μg/ml equivalent of HPMA-ZnPP and free ZnPP (with or without addition of 2 μg/ml of HPMA). Fluorescence polarization (P) values were measured (Ex. 420 nm; Em. 590 nm). See text for calculation. (C) Cleavability of HPMA-ZnPP (2.5 mg/ml) dissolved in 10 mM NaOH with or without 40% DMSO at 50 °C was examined. Cleaved free ZnPP was measured by HPLC detected by absorption at 422 nm. (D) The apparent hydrodynamic diameter of HPMA-ZnPP micelles or parental HPMA was measured by using dynamic light scattering. HPMA-ZnPP micelles (D-i) or parental HPMA polymer (D-ii) was dissolved in PBS (pH 7.4) at a concentration of 1 mg/ml. (E) Transmission electron micrograph of HPMA-ZnPP. The micelle image and HPMA-ZnPP size were analyzed via transmission electron microscopy. The inset shows high magnification image. See text for detail. (F) UV/VIS absorption spectra of HPMA-ZnPP dissolved in DMSO or PBS containing 9 M urea or 0.5% of Tween 20. (G), (H) Fluorescence spectra of 10 μg/ml HPMA-ZnPP in the presence of various concentration of Tween 20 (G), or Urea (H).

2,2,6,6-tetramethyl-4-piperidone (4-oxo-TEMP) and light-irradiation. We measured the difference in $^1O_2$ generation in both micellar and disintegrated HPMA-ZnPP forms. When micellar HPMA-ZnPP was dissolved together with 20 mM 4-oxo-TEMP in PBS (pH 7.4) and light-irradiated, it generated no $^1O_2$ (Fig. 2A). However, in the presence of 0.5% Tween 20, its $^1O_2$ generating capacity was observed, where HPMA-ZnPP is disintegrated (Fig. 2A). Addition of sodium azide, a $^1O_2$ scavenger, clearly suppressed the triplet signal of 4-oxo-TEMPO (the $^1O_2$-4-oxo-TEMP adduct) (data not shown). These results agree with those of fluorescence spectroscopy and quenching of HPMA-ZnPP micelles in PBS or aqueous systems (Fig. 1G). Free ZnPP showed a similar character to HPMA-ZnPP micelles, indicating that free ZnPP will aggregate and π–π stacking will be formed in aqueous solution, which contributes to the suppression of singlet oxygen upon light-irradiation (Fig. 2B).

3.5. Cytotoxicity of HPMA-ZnPP

Free ZnPP had an IC_{50} value of about 10 μg/ml, whereas that of HPMA-ZnPP micelles was more than 100 μg/ml of ZnPP equivalent (Fig. 2B). However, with light irradiation, both free ZnPP and HPMA-ZnPP conjugates showed markedly increased cytotoxicity; 1.0 J/cm^2 light (blue fluorescent light; Philips, Eindhoven, Netherland) with an irradiation peak at 420 nm enhanced both cytotoxicity 10–20 times {(free ZnPP, IC_{50}<1.0 μg/ml) and (HPMA-ZnPP, IC_{50} to 5 μg/ml)} (Fig. 2B).

We then examined that the contribution of cytotoxic effect of HPMA-ZnPP induced by light-irradiation is attributable to whether intracellular or extracellular drugs. In one set of assay, light irradiation was applied without a medium change, so that the drug was accessible from outside the cells; in another set of assay, we changed the medium to fresh medium without the drug, so that the drug existed primarily inside the cells. The results showed that medium replacement without the drug caused a slight decrease in cytotoxicity (Fig. 2C), which suggests that intracellular uptake of HPMA-ZnPP was the main cause of light irradiation-induced cytotoxicity.

3.6. Stability of HPMA-ZnPP micelles: lecithin induces disintegration of HPMA-ZnPP

As Figs. 1G and 2A show, HPMA-ZnPP in the intact micellar form, demonstrated the least fluorescence, did not generate $^1O_2$. Thus, to

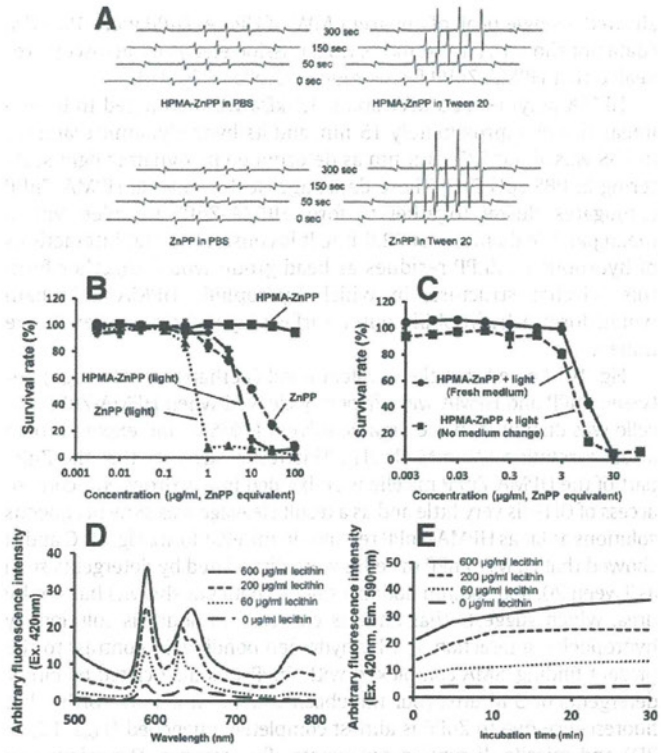

Fig. 2. Cytotoxicity of HPMA-ZnPP with light-irradiation via singlet oxygen generation. (A) ESR spectra for HPMA-ZnPP (upper panel) and ZnPP (lower panel) dissolved in PBS or in PBS containing 0.5% Tween 20 plus light irradiation for the indicated times. $^1O_2$ generated here was captured by 4-oxo-TEMP, and triplet 4-oxo-TEMPO signal due to $^1O_2$ was detected by ESR spectra. HPMA-ZnPP with Tween 20 plus light exposure considerably enhanced $^1O_2$ generation in an exposure-time-dependent manner. (B) HeLa cells, plated in 96-well plates, were treated with increasing concentrations of ZnPP or HPMA-ZnPP for 72 h. At 24 h after treatment, cells were irradiated with light and were incubated for another 48 h. The MTT assay was used to quantify surviving cells, as a ratio of the surviving fraction to the untreated control. Values (%) are means surviving cells ± s.d. (C) Effect of medium change and light induced toxicity against HeLa cells in culture. Here fresh medium was replaced for spent medium to remove free ZnPP or HPMA-ZnPP and light was irradiated. Cell survival was quantified as in Fig. 2A. (D) Disintegration of HPMA-ZnPP micelles at 10 μg/ml as determined by fluorescence spectra in the presence of increasing concentrations of egg lecithin at 25 °C for 30 min. (E) Disintegration of HPMA-ZnPP at 10 μg/ml as determined by increasing concentrations (60–600 μg/ml) of lecithin and fluorescence intensity at 25 °C for indicated times.

exhibit light-induced cytotoxicity, HPMA-ZnPP micelles must be disintegrated after cellular internalization. We thus examined the effect of cellular components; cell membrane and constituents of the lipid bilayer such as lecithin. Interestingly addition of lecithin disintegrated HPMA-ZnPP micelles as seen by the increase of fluorescence intensity (Fig. 2D). We recently reported that SMA-ZnPP underwent disintegration in cells, which was caused by the cell membrane and its component lecithin [25]. We found that fluorescence intensity of HPMA-ZnPP micelles clearly increased after addition of lecithin in a dose- and time-dependent manner (Fig. 2D, E). The same was seen after addition of cell membrane fractions of tumor and liver (data not shown).

3.7. Antitumor activity of HPMA-ZnPP in vivo

The antitumor effect of HPMA-ZnPP micelles was examined with S-180 tumor in mice. After 24, 48 and 72 h i.v. injection of HPMA-ZnPP micelles, tumors on the dorsal skin were irradiated with xenon light (20 mW/cm^2; 400–800 nm) for 5 min. Tumor sizes of two control groups which one without drug, and the other treated with HPMA-ZnPP micelles but without light irradiation increased; however, the tumor size in the group administered with the drug plus light-irradiation was reduced significantly (Fig. 3).

3.8. Cell uptake of HPMA-ZnPP

Consistent with our previous report [25], tumor cells internalized free ZnPP efficiently; however, far less HPMA-ZnPP was internalized, only about 2.5% of free ZnPP, at least up to 6 h of incubation (Fig. 4A). HPMA-ZnPP internalization was also suppressed at a low temperature (4 °C), which suggests that HPMA-ZnPP was internalized via the endocytic pathway (Fig. 4B).

3.9. Pharmacokinetics, organ distribution of HPMA-ZnPP after i.v. administration

We quantified the concentration of free ZnPP and HPMA-ZnPP micelles in the blood after i.v. injection. Free ZnPP was rapidly cleared from the systemic circulation; however, HPMA-ZnPP micelles remained in the circulation for much prolonged time, i.e. $t_{1/2}$ in plasma was about 24 h (Fig. 4C). Examination of the organ distribution of HPMA-ZnPP micelles 24 and 48 h after i.v. injection demonstrated marked accumulation of HPMA-ZnPP micelles in the tumor as well as in the liver at 24 and 48 h (Fig. 4D). In contrast, free ZnPP was found mostly in the liver, and less in the spleen, and not in the tumor (Fig. 4E). The amount of HPMA-ZnPP micelles accumulated in tumor was about 10 times more than that in the lung, kidney and heart (Fig. 4D).

3.10. In vivo fluorescence imaging after i.v. injection of HPMA-ZnPP

Fluorescence imaging using the in vivo fluorescence imaging system (IVIS Lumina-XR) confirmed the selective accumulation of HPMA-ZnPP micelles in tumor. At 24 h after i.v. injection of HPMA-ZnPP micelles, preferential fluorescence of tumor tissue was observed by excitation at 430 ± 15 nm (Fig. 5A, cf. 5A′). Furthermore, when we examined each dissected tissue, only tumor tissue fluoresced, while little appreciable fluorescence of normal tissues including the kidney, liver, lung and skin (Fig. 5B, cf. 5B′). Regardless of the accumulation of HPMA-ZnPP and free ZnPP in the liver, showed in Fig. 4D and E, fluorescence at the liver was unremarkable. This discrepancy of least fluorescence of the liver may be attributed to the high content of heme protein in the liver, which might disturb the transmission of excitation light and/or absorb the fluorescence emission, thus least fluorescence was detected in the liver. These data suggest that HPMA-ZnPP micelles can selectively accumulate in tumor tissue and it can be used for sensitive visualization

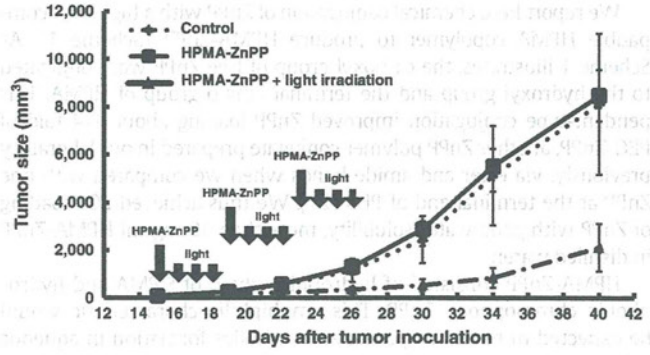

Fig. 3. Light-irradiation induced antitumor activity of HPMA-ZnPP. HPMA-ZnPP was administered at 15 mg of ZnPP per kg equivalent followed by xenon light-irradiation at the indicated times. S-180 tumor volume (mm3) was calculated as $(W^2 \times L)/2$, where L = longitudinal and W = width of the tumor.

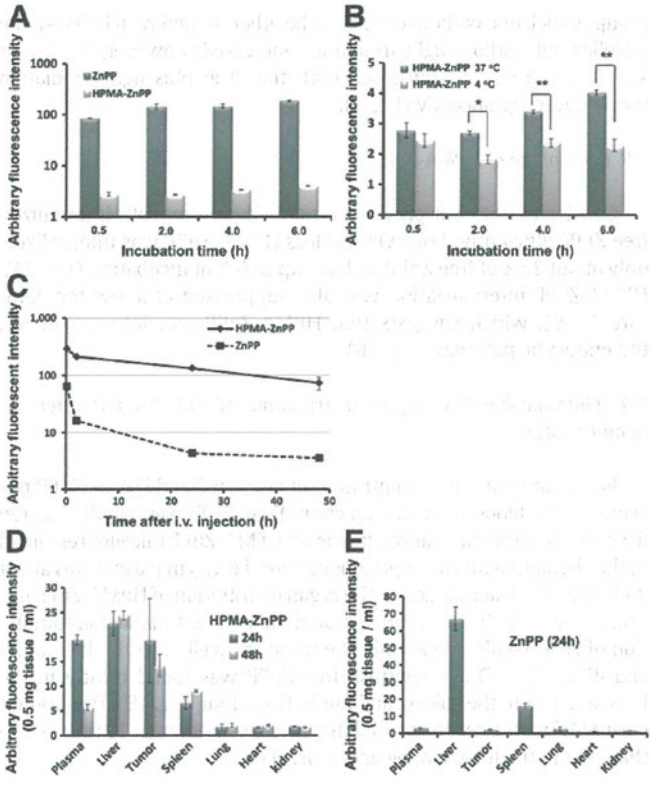

Fig. 4. Intracellular uptake, in vivo pharmacokinetics and body distribution of HPMA-ZnPP micelle. (A) Cell uptake of HPMA-ZnPP and free ZnPP by HeLa cells. ZnPP or HPMA-ZnPP (20 μg/ml ZnPP equivalent dose) was administered for the indicated time periods. After cells were washed, intracellular ZnPP or HPMA-ZnPP was extracted in ethanol, and quantified by fluorescence intensity of ZnPP and HPMA-ZnPP was measured by fluorescence spectroscopy. (B) Effect of temperature for cell uptake of HPMA-ZnPP. The methods used as same as in (A) above. Values are means ± s.d. $^{**}P<0.01$ and $^{*}P<0.05$, significant differences, according to Student's t-test. (C) Blood profile of free ZnPP or HPMA-ZnPP at 18 mg of ZnPP equivalent per kg was injected i.v. into S-180 tumor-bearing mice. ZnPP concentration was determined by fluorescence intensity. (D) (E) Tissue distribution of HPMA-ZnPP and free ZnPP at 24 and 48 h after injection of 15 mg of ZnPP equivalent/kg of (D) HPMA-ZnPP, or (E) free ZnPP. Mice were sacrificed and HPMA-ZnPP or ZnPP in each tissue was extracted with DMSO and quantified as in (C).

of tumor with use of the appropriate spectroscopic system, which simultaneously exerting therapeutic effects via generation of $^1O_2$.

4. Discussion

We report here chemical conjugation of ZnPP with a highly biocompatible HPMA copolymer to produce HPMA-ZnPP (Scheme 1). As Scheme 1 illustrates, the carboxyl group of free ZnPP was conjugated to the hydroxyl group and the terminal amino group of HPMA. This pendant-type conjugation improved ZnPP loading about 3–4 fold of PEG-ZnPP, another ZnPP polymer conjugate prepared in our laboratory previously, via ester and amide bonds when we compared with one ZnPP at the terminal end of PEG [21]. We thus achieved 20% loading of ZnPP with good water solubility, more than 30 mg/ml HPMA-ZnPP in distilled water.

HPMA-ZnPP consisted of hydrophilic chain of HPMA and hydrophobic chromophore, ZnPP. This amphiphilic characteristic would be expected to result in spontaneous micelles formation in aqueous solution. The apparent hydrodynamic diameter of HPMA-ZnPP micelles in aqueous solution exhibited a single peak distribution having mean particle diameter of 82.8 ± 41.8 nm as determined by dynamic light scattering (Fig. 1D-i, -ii), and Sephacryl S-300 chromatography showed a single peak of apparent MW of HPMA-ZnPP were 198-kDa (data not shown). Furthermore, transmission electron microscopy revealed that HPMA-ZnPP forms round micelles (Fig. 1E).

HPMA polymer at a MW about 12-kDa was estimated to have a linear size of approximately 15 nm, and its hydrodynamic diameter in PBS was about 5.6 ± 1.9 nm as determined by dynamic light scattering in PBS (pH 7.4). These data suggest that several HPMA-ZnPP conjugates cluster together to form HPMA-ZnPP micelles with a mean particle diameter of 82.8 nm. It is considered that interactions of hydrophobic ZnPP residues as head group would together form this micellar structure, in which hydrophilic HPMA tail chain would form a hydrophilic outer surface layer facing water in the milieu.

Fig. 1C showed that the covalent bond (perhaps ester linkage) between ZnPP and HPMA was efficiently cleaved when HPMA-ZnPP micelle was disrupted in the organic solvent (DMSO) and exposed to an alkaline solution (10 mM NaOH). This result suggests that the ZnPP part of the HPMA-ZnPP micelle is embedded in a hydrophobic core, so access of OH− is very little and as a result cleavage was slow in aqueous solutions as far as HPMA-ZnPP remains in micellar form. Fig. 1F, G and H showed that HPMA-ZnPP micelles were dissociated by detergents such as Tween 20, and sodium dodecyl sulfate (data not shown) but not by urea, which suggests that ZnPP is clustered in aqueous solution by hydrophobic interaction, not by hydrogen bonding. In contrast to the present finding, SMA complexed with ZnPP was dissociated by either detergents or 9 M urea (our unpublished data). It is noteworthy that fluorescence due to ZnPP is almost completely quenched (Figs. 1G, H, 2D) and micelle disruption regenerates fluorescence. Dissociation of HPMA-ZnPP micelles by cell-membrane components or lecithin also led to regeneration of fluorescence as indication of micellar disruption in the cells. Furthermore, generation of $^1O_2$ by light irradiation can be achieved more effectively when the micelles were disintegrated (Fig. 2A). This mean when micelles are in circulation they do not emit fluorescence nor $^1O_2$.

The molecular target of ZnPP, ie, HO-1 is located in the endoplasmic reticulum in the cells, thus ZnPP micelles must be internalized by cells in order to exert HO-1 inhibition which leads to cell death due to increased oxystress [25–28]. We recently showed that SMA-ZnPP was efficiently internalized by cells and exhibited cytotoxicity comparable to that of native free ZnPP; in contrast PEG-ZnPP showed much slower intracellular uptake thereby showed little cytotoxicity [25]. We found that intracellular uptake of HPMA-ZnPP was much slower than that of free ZnPP (Fig. 4A) and that HPMA-ZnPP by itself showed little cytotoxic activity against HeLa cells in vitro; even at 100 μg/ml ZnPP equivalent, unless light irradiation was applied (Fig. 2B). This low cytotoxic effect may be explained by low HO-1 inhibitory activity in the cells. HPMA-ZnPP micelles exhibited less than 10% of HO-1 inhibitory activity compared to ZnPP in a cell-free system (data not shown). The reason for this low activity may be that ZnPP is not available to interact with HO-1 because ZnPP may be stacked together in the inner core of the HPMA-ZnPP micelles. This hypothesis agrees well with our observation illustrated in Fig. 1C; DMSO disintegrated the micellar form of HPMA-ZnPP, and thus micelles become single HPMA-ZnPP chain and its ester bonding may be hydrolyzed by alkaline (OH−). Thus, HPMA-ZnPP micelles alone were not expected to exhibit anticancer activity. Consistent with this interpretation and expectation, HPMA-ZnPP alone showed no antitumor activity in vivo against S-180 tumor in mice (Fig. 3).

In contrast to above observation, however, light-irradiation greatly enhanced the cytotoxic effect of HPMA-ZnPP micelles in in vitro and in vivo (Figs. 2B and 3). In HPMA-ZnPP micelles, ZnPP probably forms a π–π stacked structure, and excited fluorochrome dissipates the energy, so neither fluorescence nor $^1O_2$ formation occurs. However, when micelles are disintegrated by detergents such as Tween 20, HPMA-ZnPP can generate $^1O_2$ under light irradiation (Fig. 2A). Consequently, we found that HPMA-ZnPP exerted cytotoxicity with light-irradiation. These results indicate that HPMA-ZnPP micelles may exist as a

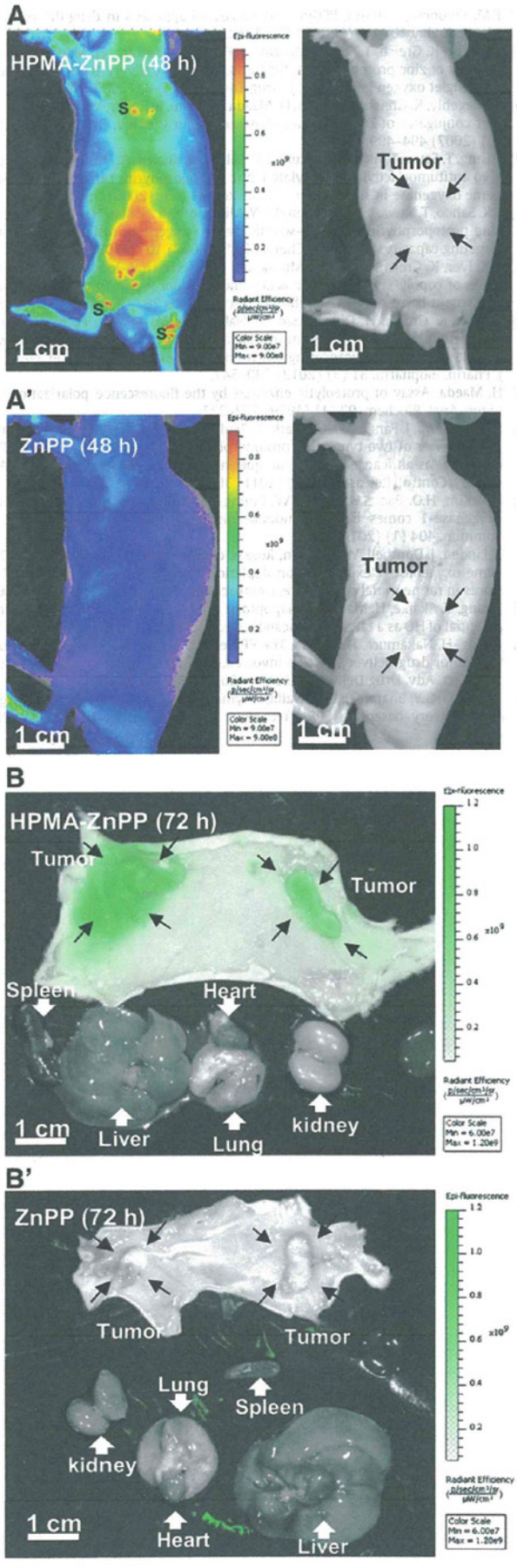

disintegrated form in the cells after intracellular internalization. We recently found that SMA-ZnPP undergoes disintegration in cells, which is caused by the cell membrane component lecithin as described [25]. We therefore anticipated that HPMA-ZnPP would be also disintegrated, as we demonstrated by adding lecithin (Fig. 2D, E).

The first critical step in selective delivery of anticancer drugs to tumors is to utilize the EPR effect. Biocompatible macromolecules of more than 40 kDa (size above 10 nm) with a neutral to slightly anionic charge are expected to accumulate in tumors via the EPR effect [9–11,29,30]. As described above, HPMA-ZnPP micelles exhibited a mean hydrodynamic diameter of about 80 nm with a zeta potential of +1.12 mV. These data indicate that HPMA-ZnPP micelles would be preferentially accumulated in tumors by EPR effect-driven mechanism.

We found that the blood half-life of HPMA-ZnPP micelles was markedly longer (>40 times) than that of free ZnPP and thus HPMA-ZnPP micelles accumulated about 10 times more in tumor than in lung, kidney and heart (Fig. 4D, E). This tumor accumulation property of HPMA-ZnPP is superior to our previous report on ZnPP micelles, i.e. SMA-ZnPP and PEG-ZnPP, having tumor/normal tissue (lung, kidney and heart) ratio of approx. 0.8–1 and 2–3 respectively [20,23]. Because of a slower intracellular uptake and lower HO-1 inhibition, HPMA-ZnPP alone showed no appreciable antitumor activity even with excessive tumor accumulation of HPMA-ZnPP (approximately 5–10 times greater than the lung or kidney, i.e. 200–300 μg/g of tissue).

Of greater interest in conjunction with fluorescence endoscopy, we found that HPMA-ZnPP micelles may be useful as a fluorescence tumor imaging probe. It emits fluorescence and produce $^1O_2$ upon light irradiation (Figs. 1G and 2A). Thus, HPMA-ZnPP micelles can be used as fluorescent nanoprobes in fluorescence endoscopy also for probe for PDT.

A xenon light source, which is usually used in conventional endoscopy, can be readily utilized in this fluorescent method. Xenon light used in the endoscope emits light with a wide spectral wavelength range, from 400 to 750 nm, so any fluorescent probe can be adapted as described here. Near-infrared light has been thought to be more useful because of better tissue penetration, although heat that is generated causes serious inconvenience. The present results in mice, however, demonstrated tumors implanted in mice readily detectable, and indicate that superficial tumors such as ductal tumors as esophageal or colonic tumor can be detected similarly. We believe therefore that the ductal tumors such as esophageal, gastric or cavity tumors of colon, uterine and urinary bladder or even abdominal and pleural cavity are ideal for application of this fluorescence endoscopy. Furthermore, the present results suggest an effective PDT by using conventional endoscopy equipped with xenon lamp would warrant noninvasive highly sensitive theranostic modality for solid tumor. Studies along this line are under way in our laboratory.

Acknowledgments

Support from the Ministry of Health, Labour and Welfare (MHLW), Japan for Cancer Specialty Grant for Hiroshi Maeda (2011–2014) and from Matching Fund Subsidy for Private Universities from the Ministry of Education, Culture, Sports, Science and Technology (MECSST), Japan, are acknowledged. We also acknowledge the grant support of GA AV CR, no. IAAX00500803, Czech Republic for Karel Ulbrich.

Fig. 5. In vivo fluorescence imaging of tumors using HPMA-ZnPP. (A) (A′) Whole-body fluorescent views of tumor-bearing mice after injection with HPMA-ZnPP (A) and free ZnPP (A′), respectively. Images were obtained 48 h after i.v. drug injection (both at 15 mg/kg ZnPP equivalent). (B) (B′) Dissected tissues of mice corresponding to (A) and (A′) under fluorescent light, with images obtained at 72 h after i.v. injection. Only tumor nodules in (A) and (B) are fluorescent.